Development of an equatorial carbonate platform across the Triassic-Jurassic boundary and links to global palaeoenvironmental changes (Musandam Peninsula, UAE/Oman)

Martin R. Hönig[1]*, Cédric M. John[1], Christina Manning[2]

[1] Qatar Carbonates and Carbon Storage Research Centre, Department of Earth Science and Engineering, Imperial College London, Prince Consort Road, London SW7 2BP, United Kingdom

[2] Department of Earth Sciences, Queens Building, Royal Holloway University of London, Egham TW20 0EX, United Kingdom

* corresponding author (martin_hoenig@hotmail.com)

Highlights

- A shallow-marine carbonate system, studied vertically and laterally, across the Triassic-Jurassic transition from the palaeoequator is presented.
- The vertical stacking pattern is controlled most likely by relative sea level changes.
- No clear evidence for a biocalcification crisis or ocean acidification across the Triassic-Jurassic boundary is visible.

Keywords

Rhaetian-Hettangian, Strontium isotope stratigraphy, Carbon isotopes, Facies architecture, Ocean acidification

Abstract

The Triassic-Jurassic boundary is marked by one of the ‘big five’ mass extinctions of the Phanerozoic. This boundary event was accompanied by several carbon cycle perturbations, potentially induced by the opening of the Central Atlantic and associated volcanism, and accompanied by an ocean acidification event. Continuous carbonate successions covering this interval of environmental change are however rare. Here data from a shallow-marine equatorial mixed carbonate-siliciclastic succession is presented, that was studied on a regional scale. Four sections that are 48 km apart were examined on the Musandam Peninsula (United Arab Emirates and Sultanate of Oman). The system was analysed for its sedimentology, vertical and lateral facies changes, and stable carbon and oxygen isotopes. Strontium isotope analysis was used to determine the position of the Triassic-Jurassic boundary horizon. The studied ramp experienced an episode of demise during the Late Triassic, followed by a restricted microbialite dominated ramp, containing large amounts of siliciclastic facies. During the Latest Triassic the diverse carbonate factory revived and flourished across the Triassic-Jurassic boundary. No clear evidence for a biocalcification crisis or an ocean acidification event across the Triassic-Jurassic boundary is visible. Lateral facies heterogeneities can be observed across the studied interval, attributed to hydrodynamic activity, including tropical storms, crossing the extensive shelf area. Although evidence for synsedimentary tectonic activity is present, the vertical stacking pattern is largely controlled by changes in relative sea level. The refined chronostratigraphy accompanied by the detailed environment of deposition analysis allows for a refinement of the regional palaeogeography. The neritic equatorial carbonate ramp has archived a negative carbon isotope excursion preceding the Triassic-Jurassic boundary that has also been reported from other study sites. The lack of evidence for a biocalcification crisis across the equatorial Triassic-Jurassic boundary indicates that the Tethys did not experience a distinct global acidification event.

1. Introduction and aims

The Triassic-Jurassic transition is accompanied by one of the major mass-extinctions of the Phanerozoic, and is marked by drastic biotic and environmental changes (e.g. Hesselbo et al., 2007) preceded by a carbon cycle perturbation (Hesselbo et al., 2002). This perturbation of the carbon cycle is synchronous with the eruption of the Central Atlantic Magmatic Province (CAMP), producing large amounts of CO_2 and associated volcanic volatiles (Cohen and Coe, 2002; Marzoli et al., 2004). Ocean acidification as the result of the exhalation of CO_2 has been suggested as the main cause for the mass extinction and the associated crisis (Hautmann et al., 2008; Greene et al., 2012, Hönisch et al., 2012; Ikeda et al., 2015). The Arabian Peninsula was covered by an extensive carbonate platform during most of the Mesozoic. The sedimentary rocks of the Arabian Platform have the potential to serve as excellent archive for palaeoenvironmental change. It has however been postulated that a significant stratigraphic gap exists between the Triassic and the Jurassic sequences on most of the Arabian Peninsula, due to erosion or non-deposition (e.g. Al-Husseini, 1997; Sharland et al., 2001; Ziegler 2001). In Oman it has therefore only been possible to study the Upper Triassic shallow-water platform (Bernecker, 2005; 2007), the Liassic shallow-water platform, unconformably overlying the Triassic (Bendias and Aigner, 2015) or the deep-sea record of the Upper Triassic to Lower Jurassic interval (Blendinger, 1988; Blechschmidt et al., 2004). The Musandam Peninsula hosts the stratigraphically most complete shallow carbonate platform section across this time interval on the Arabian Platform, although the exact stratigraphic boundary positions and hiatuses within the Late Triassic and Early Jurassic sequences in this region still remain unclear (Maurer et al., 2008; 2015). The Musandam Peninsula was located at an equatorial position during the Late Triassic to Early Jurassic interval (Tanner et al., 2004; Golonka, 2007). A continuous sedimentary record across the Triassic-Jurassic boundary is rare (Greene et al., 2012 and references therein), and so the carbonate platform of the Musandam Peninsula offers a unique opportunity to examine a carbonate platform at an important palaeogeograpic location, potentially affected by major environmental changes across the Triassic-Jurassic boundary.

The aims of this study are: (1) to construct a robust chronostratigraphic framework for the Upper Triassic to Lower Jurassic carbonate sequences on the Musandam Peninsula and

(2) to examine the evolution of an equatorial carbonate system across an interval of major global environmental change. These findings are then used to evaluate implications for the regional palaeoceanography and assess factors controlling the development of the carbonate system at the Triassic-Jurassic boundary.

2. Study area and geological setting

Four sections were selected for this study that are located on the Musandam Peninsula (Fig. 1A). The southern part of Musandam Peninsula is part of the United Arab Emirates (UAE) and the northern area is part of the Sultanate of Oman. The Musandam Mountains on the peninsula form the north western extension of the Oman Mountains and contain a well preserved, ~3 km-thick succession of shallow-water carbonates (Maurer et al., 2009). The eastern margin of the Arabian Plate was tectonically passive during the Permian and the Mesozoic. The overall relative tectonic quiescence was interrupted by two events, one during the Late Cretaceous when ophiolites were obducted on the Arabian plate, and the second one during the Late Oligocene – Early Miocene when the Oman and Musandam Mountains were formed during an initial collision phase of the Zagros orogeny (Glennie, 2005; Searle et al., 2014). From the Pliocene onwards the eastern margin of the Arabian platform was in an active continental setting and the Arabian plate is currently being subducted beneath the Eurasian Plate (Sharland et al., 2001; Searle et al., 2014).

The area of the Musandam Peninsula was located at an equatorial position during the Late Triassic to Early Jurassic interval (Tanner et al., 2004; Golonka, 2007). The area was covered by a shallow-marine carbonate platform during the Late Triassic and Early Jurassic (Ziegler, 2001) (Fig. 1B). To the north, more open-marine conditions prevailed. Terrigenous conditions existed to the south, with the coastline towards the west running roughly parallel to its present day location (Ziegler, 2001). Most of the UAE, Oman and Qatar were characterised by terrigenous to marginally marine environments, where shallow-marine clastics, evaporites and coastal and deltaic sediments were deposited (Al-Husseini, 1997; Ziegler 2001).

The four sections are 48 km apart (Fig. 1A). The “Wadi Naqab section” lies on the

northern side of Wadi Naqab, 13 km southeast of the city of Ras-Al-Khaimah (GPS coordinates of the log base: N 25°43'5.7"; E 56°05'14.1"). The "Wadi Ghalilah section" is located on the western flank of Wadi Ghalilah (GPS coordinates of the log base: N 25°58'23.1"; E 56°05'40.5"). The "Wadi Al-Ghabbah section" forms the northern extension of Wadi Sha'am, to the northeast of the city of Sha'am and is in close proximity to the border with Oman to the north (GPS coordinates of the log base: N 26°03'13.3"; E 56°08'32.6"). The "Jabal Sall Ala section" is located on the seaward facing flank of the mountain by the village Sall Ala in the Omani part of the Musandam Peninsula (GPS coordinates of the log base: N 26°01'46.6"; E 56°22'44.8".

3. Methods

The four sections were logged bed-by-bed using a Jakob's staff, and examined in the field for their sedimentary features, fossil assemblages and texture. Textural classification of carbonate facies followed Dunham (1962) and Embry and Klovan (1971). Palaeocurrent directions were measured from a cross-stratified bedset in the basal Musandam Limestone in Wadi Naqab using a geologic compass. Fist-size samples for petrography and stable isotope analysis were taken every 2 to 5 m along the vertical transects, using a geological hammer, and 51 representative thin sections were made. Half of each thin section was stained after the method described by Dickson (1965), and subsequently analysed using a transmitted light Zeiss Axioskop 40 microscope (plain and polarised light).

Stable isotope measurements were performed in the Qatar Stable Isotope Laboratory at Imperial College London. All measurements were performed on micrite as it is the most common carbonate phase, and thin section analysis could be used to check the purity of the micrite. Where it was not possible to sample the micrite phase, a bulk sample was analysed. A total of 148 sample powders were obtained using an electrical dental drill, carefully avoiding veins, fossils and recrystallized sections. Approximately 100 to 230 µg (one sample with a relatively low $CaCO_3$ content) of sample powder were dissolved with 105 % orthophosphoric acid at 70 °C in a Kiel IV carbonate device, and the resulting CO_2 gas was measured on a

Thermo MAT 253 mass spectrometer**.** Data were corrected according to measurements of the international standard NBS 19 and an in-house standard (ICM, Imperial College Carrara Marble and processed for carbon and oxygen isotope drift using the software Easotope (John and Bowen, 2016). Stable isotope values are reported using the standard δ notation relative to the VPDB (Vienna Pee Dee Belemnite) standard. External precision for ICM (one standard deviation) on carbon and oxygen is better than 0.05 ‰ and 0.08 ‰, respectively. The precision for duplicate and triplicate sample measurements (one standard deviation) is better than 0.05 ‰ for carbon and better than 0.14 ‰ for oxygen.

The strontium isotope analyses ($^{87}Sr/^{86}Sr$) were carried out at the Royal Holloway University of London on selected oysters and brachiopods. The brachiopods were screened for diagenetic alteration prior to the analysis at Imperial College London using petrographic and cathodoluminescence (CL) microscopy. A CITL Cathodoluminescence Mk5-2 stage mounted on a Nikon Eclipse 50i microscope was used. Operating conditions for the CL microscope were about 270 µA and 14 kV. Samples were acidified for one hour at 80 °C using 5 % HNO_3 solution. Strontium was then separated from the solution using EichromSr-spec resin and then loaded on single Re filaments with a TaF emitter. The $^{87}Sr/^{86}Sr$ analyses were determined using the multidynamic procedure of Thirlwall (1991) and analysed on an Isotopx Phoenix Thermal Ionisation mass spectrometer. The standard SRM 987 analysed alongside samples gave a mean of 0.710237+-0.000006 (2sd, N=3) (Appendix), within error of the long-term mean of 0.710234+-11 (2sd, N=177).

4. Chronostratigraphic framework

Consensus seems to prevail that Upper Triassic and a large portion of Lower Jurassic sediments are not preserved on much of the Arabian Platform due to erosion, or were never deposited due to exposure during a sea level lowstand (e.g. Alsharhan and Nairn, 1994; Al-Husseini, 1997; Le Nindre et al., 2003; Bendias and Aigner, 2015). Liassic deposits of Toarcian age occur on parts of the Arabian Shield due to a transgression and the subsequent creation of accommodation (Al-Husseini, 1997). On the Musandam Peninsula, a more

complete stratigraphic record of the Triassic and Jurassic is present. The Triassic period is only missing parts of the Carnian and Norian (Maurer et al., 2008). The Jurassic sedimentary record is missing parts of the Hettangian and Sinemurian and parts of the Toarcian, the Aalenian and the Tithonian (de Matos, 1997; de Matos and Walkden, 2000).

The four sections comprise the top Sumra Member, the Sakhra and Shuba Members as well as the basal Musandam Limestone (Fig. 2; 3A). The former are the upper members of the Ghalilah Formation and the Musandam Limestone forms the Lower Musandam Formation. The three members as well as the underlying Asfal and Sumra Members were originally described by Hudson (1960) and attributed to the Triassic. Glennie et al. (1974) later revised this and dated the Sakhra and Shuba Members as Early Jurassic, based on a single *Orbitopsella* specimen, thus extending the Ghalilah Formation into the Jurassic. This was supported by Maurer et al. (2008; 2015) and followed by Al-Suwaidi et al. (2016) based on the last occurrence of Rhaetian corals in the uppermost Sumra Member and the absence of fossils in the Sakhra and Shuba Members, which Maurer et al. (2008; 2015) attribute to the end-Triassic mass extinction. De Matos et al. (1994) and de Matos (1997) studied the Jurassic stratigraphy in Wadi Naqab extensively and, based on the macrofossil assemblage described previously by Hudson and Jefferies (1961) and the stratigraphic study by Metwally and Ali (1992), identified the contact between the Shuba Member and the basal Musandam Formation as the Triassic-Jurassic boundary at Wadi Naqab. It is noteworthy that Metwally and Ali (1992) assign an Early Jurassic age to the “cliff-forming limestones” (presumably the basal Musandam limestone and not the Sakhra limestone, since the latter is only approximately 25 m thick (Hudson, 1960)) based on a macrofossil assemblage containing the ammonoid *Tragophylloceras numismale* and the echinoid *Scaptodiadema*. The ammonite *T. numismale* points to a Pliensbachian age in the Euroboreal realm (Meister et al., 2012). It is furthermore noted that Maurer et al. (2008), who focused on the Permian to Triassic sequences of the Musandam Peninsula, place the Triassic-Jurassic boundary based on the last occurrence of *Retiophyllia* corals in the Upper Sumra Member, as both the Sakhra Member and most of the Shuba Member do not contain any age-diagnostic fauna. De Matos (1997) performed a detailed biostratigraphic examination of the Upper Ghalilah and the Musandam Formations in Wadi Naqab and neighbouring wadis and did not confirm the

Orbitopsella find from Glennie et al. (1974) in the Shuba Member. The Triassic-Jurassic boundary was placed within the uppermost Shuba Member based on the presence of abundant Liassic *Balanocrinus subteroides* crinoids in the basal Musandam Limestone and an assemblage of Triassic shark teeth (*Acrodus* cf. *lateralis*) and, most likely, Triassic bivalves (*Pseudoplacunopsis* sp*., Plicatula radiata, Bakevillia* sp.) encountered in a correlatable section examined in Wadi Milaha (~ 8 km north of Wadi Naqab) in the Upper Shuba Member (de Matos, 1997).

5. Results

5.1 Lithofacies associations

Nine different lithofacies associations (LF 1 to 9) were differentiated (Table 1). LF 1 comprises fenestral mud- and wackestones, containing peloids and bioclast fragments. Quartz grains as well as 2-5 cm long mudclasts are common in this facies. In some of these beds, subangular vugs with a diameter of up to ca. 15 cm are present (Fig. 3B). Some of these vugs are filled with nodular white cement, occasionally with a pink cement nucleus. Some of these vugs have irregular rims, resembling cauliflower (Fig. 3C). LF 2 comprises boundstones and mudstones containing laminae with fenestrae (Fig. 3D). The microbial laminites occur commonly as continuous beds and occasionally occur with domal structures, thus forming stromatolites. Tepee-structures are common within these laminites (Fig. 4A). The mudstones of LF 1 and 2 are frequently dolomitized. Two distinct types of crystalline dolomite occur. A fine-grained type with fine rhomb-shaped dolomite crystals (10 µm in diameter) cemented together and a coarser type where large dolomite rhombs (50 µm in diameter) float in a calcite cement matrix. LF 3 and LF 4 comprise wackestones, mudstones and packstones, containing few specimens of bivalves, gastropods, peloids, ostracods, echinoderms and dasycladalean algae fragments (*Paleodasycladus* sp., Fig. 4.3E, F). The wackestone facies is in some cases channelized (Fig. 4B). LF 4 is distinguished from LF 3 by the fact that the former contains quartz, and is occasionally partly dolomitised. LF 3 contains

no quartz grains. Bedding within the two lithofacies types is often irregular and nodular, and occasional bioturbation occurs. LF 5 has a grainstone texture, typically containing ooids and peloids (Fig. 4C). The nuclei of the ooids are mostly bioclasts, though quartz grains are also abundant. Different bivalves, such as oysters are commonly present within this facies association as well as different other bioclasts, including echinoderms. LF 5 additionally frequently contains lithoclasts and aggregate grains (Fig. 4D). It is typically cross-stratified as well as cross-laminated, and mud-drapes can be observed (Fig. 4E, F, G). LF 6 comprises diverse packstones or sometimes rudstones with a rich fossil content. The fossil content includes complete bivalve shells and fragments, and often oysters, gastropods, benthic foraminifera, ostracods, echinoderms, peloids and coral fragments. These beds have often been heavily bioturbated. The abundant ichnofossils are commonly *Rhizocorallium* and *Chondrites*. LF 7 is characterised by the presence of corals. These can occur as branching framestones, with the corals preserved in living position (Fig. 5A), massive coral heads (Fig. 5C, D) or coral debris rudstones (Fig. 5E). The matrix of the limestones around the corals is formed of ooids and large gastropods. LF 7 is in places heavily bioturbated and contains cm-sized vugs. The branching corals in the top part of the Sumra Member on the Musandam Peninsula have been identified as *Retiophyllia* corals (Maurer et al., 2008). LF 8 comprises siliciclastic facies of fine to medium sized quartz sandstones, which are typically cemented by calcite (Fig. 5B). Occasional dolomite cement is present. These sandstones are often cross-stratified and cross-laminated (Fig. 5F), exhibit nodular bedding, and sometimes show flaser-bedding, lenticular bedding as well as wave ripples (Fig. 5G) and in one case hummocky cross-lamination (Fig. 5H). Other clastic rock types included in this facies association are monomictic and polymictic conglomerates (Fig. 5I). LF 9 comprises shales and marls that are very abundant throughout the studied sections. These fine-grained sediments are brownish to grey, red and green in colour and are typically finely laminated. Bioturbation is common, mostly *Thalassinoides*.

5.2 Vertical stratigraphic stacking pattern

The base of the measured Wadi Naqab section is in the upper part of the Sumra Member (Fig. 6). It is formed of bioclastic limestones (LF 6) and coral float- and rudstones (Fig. 5C, D, E) (LF 7) interbedded with marl and shale beds (LF 9). The Sumra member is overlain by a ~ 26 m thick oolite unit (LF 5), which forms the Sakhra Member. The oolite shows abundant cross-bedding and cross-laminations. The top of this oolitic grainstone unit is marked by red staining, as well as scours and fractures, containing red mudstone and oolite clasts (Fig. 7A). The oolitic grainstone is overlain conformably by the Shuba Member. The Lower Shuba Member is dominated by microbial and fenestral limestones (LF 2), fine sand- and siltstone beds (LF 8), interbedded with marl and shale layers (LF 9). The upper half of the Shuba Member contains mainly bioclastic and oolitic limestones interbedded with marls (LF 3, 5, 6 and 9). The uppermost beds of the Shuba Member are condensed, pale brown to yellowish, ooidal grainstones, rich in oysters and crinoids (LF 5 and 6). The Shuba Member contains 19 discontinuity surfaces, which are marked by mineral crusts, red staining and occasionally by abundant bioturbation. Two of these surfaces contain desiccation cracks (Fig. 7B). The basal part of the overlying Musandam Limestones consists of a 7 m thick cross-stratified very heterogeneous (Fig. 4E, F) ooidal grainstone unit (LF 5), containing one crinoidal packstone bed (LF 6), dm thick layers of bioclastic pack- and grainstones (LF 6) and frequent 5 – 10 cm thick mudstringers (Fig. 4G). The measured palaeocurrent directions from this cross-stratified interval are NNE-SSE trending (Fig. 4E). The upper part of the section is marked by dm to 1.5 m thick mud- to wackestone beds (LF 3 and 6).

The oolites of the Sakhra Member form the basal part of the Wadi Ghalilah section (LF 5) (Fig. 6). The Sakhra Member contains one channelized bed. The channels are approximately 30 cm deep and filled with laminated mudstones (Fig. 7C). The cliff-forming Sakhra Member is overlain by the Shuba Member, which comprise in its lower part interbedded microbial boundstones (LF 2), bioclastic pack- to grainstones (LF 6) and ooidal grainstone beds (LF 5). The upper part of the Shuba Member contains microbial boundstones, fenestral mudstones (LF 2), interbedded with fine sand- to siltstones, one monomictic conglomerate bed (Fig. 4.5I) (LF 8) and marl and shale layers (LF 9). One of the fenestral mudstone beds contains small normal-fault blocks (55 m upsection, Fig. 7D). The uppermost Shuba Member contains bioclastic limestone beds with several thin oyster

packstone layers (LF 6), interbedded with marls and shales (LF 9). The topmost of these beds is a coral float- to rudstone (LF 7), with some large, massive corals in growth position (Fig. 5A). The coral limestone is overlain by several siliciclastic and quartz-rich limestone beds (LF 8 and 4). The onset of the overlying Musandam Limestone is placed where the beds are thicker and are more resistant to weathering. The lower part of the Musandam Limestone forms the top part of the logged section and comprises mudstone (LF 3 and 4) and sand- and siltstone beds (LF 8). The Shuba Member logged in Wadi Ghalilah contains 12 discontinuity surfaces of which three are marked by desiccation cracks. The Lower Musandam Limestone contains three such discontinuity surfaces.

The base of the measured Wadi Al-Ghabbah section corresponds to the top at the Sakhra Member, which forms a prominent ledge and consists of ooidal grainstone (LF 5) (Fig. 6). The basal part of the overlying Shuba Member consists of 12 m of microbial boundstones (LF 2), mudstones (LF 3) and few bioclastic limestones (LF 6). This interval is overlain by 30 m of shales and marls (LF 9), which are interbedded with dm to metre-thick limestone (LF1, 2 and 3). The mudstones of LF 1 in this interval are characterised by abundant vugs with diameters of around 10 cm, which are sometimes filled with white cement. The upper half of the Shuba Member is dominated by marl and shale beds (LF 9). These are interbedded with mainly metre-thick beds of mudstone (LF 3) and bioclastic wacke- and packstones (LF 6). A noticeable 1.05 m thick cross-stratified sandstone bed, which is overlain by a thin polymictic conglomerate, lies within this interval (60 m upsection, both LF 8). The conglomerate is only present in depressions within the top of the underlying sandstone. It consists of grey and ochre coloured mudclasts with diameters between 1 and 5 mm. Approximately 6.5 m up section a second prominent, 2.35 m thick, cross-stratified and cross-laminated sandstone bed (Lf 8) is present (67 m upsection, Fig. 5F). In its upper half it contains a horizon with lenticular bedding and internally laminated wave ripples (Fig. 5G). This bed is in parts bioturbated internally and on its surface. The top surface of the bed is a condensed layer, rich in bioclasts and coloured pale brown- to yellowish with red stained patches. The overlying Musandam Limestone above the Shuba Member is marked by thicker beds and contains an echinoid-rich wackestone (LF 3) and two very quartz-rich beds (LF 4) in its basal part. These two beds are

overlain by thickening-upwards mudstones (LF 1, 2 and 3). The Shuba Member in Wadi Al-Ghabbah contains 11 discontinuity surfaces of which one is marked by desiccation cracks.

The Jabal Sall Ala section consists of limestone beds (LF 3 and 6) interbedded with shales and marls of the Sumra Member in its basal part (Fig. 6). The uppermost Sumra Member contains two coral float- to rudstone beds with well-preserved branching corals (Fig. 5C, D, E) (LF 7) as well as two ooidal grainstone beds (LF 5). The overlying Sakhra Member is 25 m thick, and contains 5 thickening upwards, partly cross-stratified and cross-laminated ooidal grainstone beds (LF 5). The overlying Shuba Member contains microbial boundstones (LF 2) and silt- to fine sandstones (LF 8) in its lower half, interbedded with few thin shale and marl layers (LF 9). The upper half of the Shuba Member contains different types of limestone beds (LF 3, 4, 5 and 6), interbedded with shales and marls (LF 9). The basal Musandam Limestone is marked by a cross-stratified ooidal grainstone bed (LF 5), overlain by ooidal grainstone and by a relatively thick (> 3 m) bioclastic packstone bed (100 m upsection, LF 5 and 6). The Shuba Member of the Jabal Sall Ala section contains three discontinuity surfaces.

5.3 Stable carbon isotope record

The majority of $\delta^{13}C$ values from the three sections lie between -3 and 2 ‰ (Fig. 6). The $\delta^{18}O$ values lie between -7 and -1 ‰. A table containing all carbon and oxygen isotope results can be found in appendix. A cross-plot of stable isotope results from the three measured sections shows no significant trends between $\delta^{13}C$ and $\delta^{18}O$ (Fig. 8). The dataset could however be divided into two groups, one with $\delta^{18}O$ values of between 0 and -2.7 ‰ and a second group with more depleted $\delta^{18}O$ values between -3 and -8 ‰. The longest $\delta^{13}C$ record generated from samples taken from Wadi Naqab ranges from the Upper Sumra Member to the basal Musandam Limestone with the largest values corresponding to the ooidal grainstone of the Sakhra Member.

5.4 Strontium isotope stratigraphy and chronostratigraphy at Wadi Naqab

$^{87}Sr/^{86}Sr$ isotope analysis was performed oysters and a single brachiopod from Wadi Naqab (the positions of the samples are indicated in Fig. 6 and 10A). Only specimens that display little or no luminescence were selected for the Sr analysis as this implies low Mn^{2+} and Fe^{2+} concentrations (Boggs and Krinsley, 2006). The brachiopod sample (WN 193 Br3) was taken from the top of the Asfal Member (the lowest member of the Ghalilah Formation) approximately 40 m stratigraphically below the base of the studied section. The specimens are thicker than 500 µm and the foliated texture is well-preserved (Fig. 9A, B). The sample WN 168 Oy was taken from a fossil-rich bioclastic rudstone in the top of the Shuba Member. The selected specimen is relatively thin and contains luminescent cracks (Fig. 9C, D) Samples WN TJ B2 and WN TJ B3 were taken from an ooidal grainstone bed, rich in oysters and crinoids, two beds above. The selected specimens have relatively thick shells and have a well-preserved internal foliation (Fig. 9E, F). A table containing all strontium isotope results can be found in Appendix A.4. The Asfal Member was unequivocally deposited during the Late Triassic and is therefore younger than ~232 Ma (de Matos, 1997; Maurer et al., 2008; 2015). Using the LOWESS best fit-curve by McArthur et al. (2001), the strontium isotope analysis yields in a numerical maximum age of ~208.3 Ma for the brachiopod sample, which corresponds to the Rhaetian (Fig. 10B) (Cohen et al., 2013). The bed containing sample WN 168 Oy was deposited significantly above the bed from which the brachiopods were taken and is thus younger in age. Its measured $^{87}Sr/^{86}Sr$ value yields in a minimum stratigraphic age of ~203.8 Ma and a maximum age of ~208 Ma. Due to the shape of the LOWESS best-fit curve an unequivocal age determination using the $^{87}Sr/^{86}Sr$ value is not possible around the inferred Triassic-Jurassic boundary (dated at ~201.3 Ma, Cohen et al., 2013). The two samples WN TJ B2 and WN TJ B3, taken from the same bed, show overlapping $^{87}Sr/^{86}Sr$ values. The numerical maximum age according to the LOWESS best-fit curve is ~201.5 Ma and the minimum age is ~195.8 Ma. This theoretically implies an age difference between the bed with the two samples WN TJ B and the bed containing WN 168 Oy, separated by one bed, of between 2.3 to 12.2 Myr (Fig. 10B). Based on the texture of sample WN 168 Oy showing luminescent cracks this sample is tentatively excluded from the age determination

(Fig. 9C, D). Using the numerical age derived from the radiogenic strontium isotope analysis alone does thus not allow an unambiguous placement of the boundary.

Despite often being incomplete and prone to diagenetic alteration, the sedimentary sections from this neritic setting contain distinct shifts and has most likely archived the characteristic “initial” negative carbon isotope excursion and the following positive shift (Hesselbo et al., 2002) (Fig. 11) A lithologic control on the stable carbon isotope signal can however not be fully excluded. This is complemented by the biostratigraphic observations made by de Matos (1997) with the last occurrence of Triassic shark teeth and bivalves (see section 4 and Fig. 6) in the uppermost Ghalilah Formation. The dasycladalean algae described here (Fig. 3E, F) could only be identified at the genus level and do therefore not allow for a detailed age assignment. The genus *Paleodasycladus* has however been frequently reported from the Liassic in the western Tethys (e.g. Barattolo and Bigozzi, 1996; Di Stefano et al., 1996). The Triassic-Jurassic boundary interval is therefore placed at the transition zone between the Shuba Member and the Musandam Limestone, above the horizon containing the last Triassic taxa, based on the combined strontium-derived numerical age, the carbon isotope pattern as well as available biostratigraphic markers.

6. Discussion and implications

6.1 Environments of deposition (EOD)

Based on field observations and microfacies analysis, palaeoecological and hydrodynamic interpretations, five main environments of deposition (EODs) were identified: (i) floodplain or tidal flat, to intertidal zone; (ii) restricted, shallow-marine ramp; (iii) high-energy, shallow-marine ramp; (iv) open marine ramp and (v) subtidal middle ramp (Table 1). LF 1 and LF 2 were deposited on mudflats or tidal flats within the intertidal, shallow-marine realm. Tepee structures within the microbialite layers and desiccation cracks marking some of the discontinuity surfaces, which frequently cap these facies types, serve as evidence for regular subaerial exposure. The cauliflower-shaped vugs (Fig. 3B, C) filled with white calcite cement

that are present in some of these beds are interpreted as former evaporite nodules, which were dissolved and later filled with calcite cement. The precipitation of evaporites, such as anhydrite indicates a very shallow, intertidal and at least at times restricted or supratidal environment (e.g. Warren and Kendall, 1985). The occurrence of intertidal fenestral limestones and occasional domal stromatolites, interbedded with subtidal shales and limestones resembles the vertical stacking pattern of Lofer cycles, with the fenestral and microbial limestone facies being typical tidal flat deposits (e.g. Fischer, 1964; Satterley and Brandner, 1995; Enos and Samankassou, 1998). The finely laminated marls and shales (LF 9) are also mud- or tidalflat facies, since they are interbedded with the intertidal facies. The sandstones of LF 8 that contain wavy, and lenticular bedding (Fig. 5G) as well as cross-stratification (Fig. 5F) were most likely all deposited within the shallow-marine realm or even on mud or tidal flats. LF 3 and 4 contain little or no bioclasts, displaying a low faunal diversity, typically either bivalves, gastropods or echinoderms. LF 4 contains quartz grains, while LF 3 lacks quartz. These facies types represent a relatively restricted environment, either deposited within the shallow-marine or subtidal open ramp. No sedimentary structures could be observed to allow a more differentiated interpretation. The ooidal grainstones of LF 5 were deposited within the high-energy, shallow-marine realm. The facies contain no micrite and are typically cross-stratified and contain various bioclast fragments, such as oysters and other, unidentified bivalves, gastropods, echinoderms and lithoclasts. The coral bearing facies (LF 7) are attributed to a shallow- to more open-marine, high-energy carbonate ramp, as the corals are frequently associated with ooidal, grainy matrices and were likely to form reefs within the shallow-marine environment. The open marine EOD is dominated by lithofacies associations with diverse fossil assemblages such as pack- and rudstones of LF 6, containing bivalves, gastropods, benthic foraminifera, ostracods, echinoderms, oysters, peloids and coral fragments. The ichnofossils *Rhizocorallium* and *Chondrites* point to a slightly deeper marine EOD, compared to the restricted and fossil-lean deposits of LF 3 and 4. The hummocky cross stratification in one sandstone bed in the top Shuba Member at Wadi Al-Ghabbah is interpreted as being produced by storm-induced currents. These sands were most likely deposited between storm- and fair-weather wavebase. The finely laminated shales and marls of LF 9, often exhibiting nodular bedding and bioturbation (typically *Thalassinoides*)

are deposits of a relatively deep, calm environment, and thus represent the deepest deposits within the studied sections.

6.2 Sequence stratigraphic framework

The sequence stratigraphic scheme used in this study follows concepts proposed by Strasser et al. (1999). The workflow allows for a descriptive analysis of vertical stacking patterns in shallow environments, especially for mixed, carbonate-clastic systems. The high-resolution analysis groups units into sequences based on vertical facies trends and interpreted bathymetric changes. This has proven useful when age constraints are relatively loose and the exact duration of sequences is difficult or impossible to assess, and has been applied in various studies (e.g. Immenhauser et al., 2004; Amour et al., 2013; Gomez and Astini, 2015). Two different scales of sequences were recognised within the studied strata based on the cyclical, vertical facies evolution. Small-scale sequences are typically a few metres to tens of metres thick, and the large-scale sequences have thicknesses of maximum 30 m. When the vertical facies evolution indicates deepening-upwards, the sequence is interpreted to record increasing sediment accommodation and a relative sea level rise, while a relative shoaling-upwards sequence is interpreted to have recorded decreasing accommodation and a relative sea level fall. Sequence boundaries were placed at surfaces containing evidence for breaks in sedimentation, such as discontinuity surfaces, some showing evidence for subaerial exposure such as desiccation cracks and palaeokarsts, or where breaks in the trend of relative sea level change are evidenced. The application of the described workflow allows the identification of sequences for the four studied sections as follows (Fig. 12): The measured Wadi Naqab section is divided here into seven sequence sets. Each of these sequence sets consists of a deepening and a shoaling-upwards sequence. The top of the Sakhra Member oolites is strongly karstified and thus for example forms a sequence boundary (Fig. 7A). De Matos (1997) has previously described the Jurassic succession in Wadi Naqab. The sequence “He1”, corresponding to the basal Musandam Limestone (de Matos, 1997), is approximately equivalent to the top two and a half sequences in the new sequence stratigraphic scheme presented here. The Wadi Ghalilah section consists of six and a half

sequence sets. The Wadi Al-Ghabbah section consists of eight complete sequence sets. The basal oolitic unit marks the top of a shoaling-upwards sequence and the uppermost beds of the section mark the beginning of a deepening-upwards sequence. The Jabal Sall Ala section consists of seven sequence sets. Sequences were grouped into lager order sequences in a composite sequence stratigraphic framework for all four studied sections (Fig. 12). This results in a shoaling-upwards sequence ranging from the Sumra Member to the top of the Sakhra Member. The overlying Shuba Member and Musandam Limestone are interpreted as a deepening upwards – shallowing-upwards sequence set, with the relatively deepest deposits within the top Shuba Member.

6.3 Regional correlation

The four sections are correlated based on a combined stratigraphic approach. The Wadi Naqab section is used as regional reference section as its chronostratigraphic age has been constrained by bio- and isotope stratigraphy. All three $\delta^{13}C$ curves show broad negative trends in their lower parts followed by a positive shift with amplitudes of 3.5 – 4 ‰. The relatively heaviest value at Wadi Naqab (WN 3 – WN 4, Fig. 6) comes from to the basal Musandam Limestone and the Triassic-Jurassic transition zone. The heaviest $\delta^{13}C$ values following the 3.5 – 4 ‰ shifts at Wadis Ghalilah (WG 2 – WG 3, Fig. 6) and Al-Ghabbah (within WA 4, Fig. 6) are interpreted to correspond to the heaviest value recorded at Wadi Naqab. The heavy $\delta^{13}C$ values at Wadis Ghalilah and Al-Ghabbah occur within the basal Musandam Limestone. The Jabal Sall Ala section is correlated to the Wadi Naqab section at the Lower Musandam Limestone. This combined $\delta^{13}C$ and lithostratigraphy correlation line is used as datum in the regional correlation panel and corresponds to the Triassic – Jurassic boundary horizon (Fig. 12).

The chronostratigraphic framework established for the four sections allows for regional correlations and examination of inferred EODs, as deduced from lithofacies associations, as well as the regional correlation of sequences. The broad EODs are

continuous across the entire study window. It changes from high-energy, open marine environment to the shallow-marine, intertidal to tidal flat zone. This tidal- or mudflat EOD contains an abundant siliciclastic fraction, especially in the eastern Wadi Naqab and Jabal Sall Ala sections. The environment then shifts to open-marine, represented by diverse bioclastic limestones of the Upper Shuba Member. The Lower Jurassic is marked by open-marine and high-energy facies in the eastern sections while the western sections (Wadis Ghalilah and Al-Ghabbah) contain facies types deposited on a restricted part of the carbonate ramp. Siliciclastic as well as tidal- or mudflat facies are present within this restricted EOD that are however not continuous between the western sections. The overall thickness of the Shuba Member as well as of the recorded EODs present within that member changes markedly laterally. While the Shuba Member is approximately 50 m thick in the eastern sections (Wadi Naqab and Jabal Sall Ala sections) it is ~ 60 m thick at Wadi Ghalilah and ~ 75 m thick in Wadi Al-Ghabbah. The Wadi Al-Ghabbah section also contains more sequences than the other sections and is therefore regarded as the stratigraphically most complete out of the four sections. The general thickening towards the west could be the result of larger sediment accommodation in the west, potentially induced by an overall extensional tectonic regime, as evidenced by synsedimentary normal faults in a bed within the Shuba Member in Wadi Ghalilah (Fig. 7D), or by differential subsidence and the subsequent creation of more accommodation towards the west. Conversely local erosion in the eastern locations could account for the missing cycles. This is supported by the abundance of erosional surfaces at Wadi Naqab. The Jabal Sall Ala section however lacks these surfaces (Fig. 6). A locally different palaeotopography with a palaeolow towards the west could be postulated but is at present not possible to assess, as the base of the underlying Sakhra Member could not be measured in Wadi Al-Ghabbah.

6.4 Implications for palaeogeography

The broad palaeobathymetric configuration during the Rhaetian and Hettangian of the northeastern Arabian Peninsula shows a deepening towards the (Neo)-Tethyan ocean in the northeast (Fig. 13A). The area of the Musandam Peninsula was part of a large bay, covered

by a shallow-marine carbonate platform, with shallower clastics and evaporites being deposited in more proximal settings towards the Arabian Craton (Al-Husseini, 1997; Ziegler, 2001). Based on the findings of this study, a differentiation between the Late Triassic and the Early Jurassic is necessary as the EOD distribution markedly changed through time (Fig. 12). The Shuba Member contains multiple exposure surfaces as well as some evaporite beds in its lower half across the entire study area. The shallow-marine clastic and evaporite EOD must have extended at least to the northern end of the Musandam Peninsula during parts of the Rhaetian (Fig. 13B). This is supported by facies descriptions acquired from cores onshore and offshore of Abu Dhabi, where clastic deposits have been reported (Loufti and Sattar, 1987; Hassan, 1989). This shallow-marine clastic and evaporites EOD potentially extended as far as Iran during the Late Triassic according to facies descriptions from Alavi (2004). Since equivalent subsurface data from the Persian Gulf is scarce, this remains a hypothesis at present. The sedimentary record from the Musandam Peninsula is proposed as being more complete than that of the western Arabian Peninsula (Maurer et al., 2008) and a Late Triassic – Early Jurassic stratigraphic gap is frequently mentioned (e.g. Sharland et al., 2001). The Triassic and Jurassic facies distribution on the Musandam Peninsula is more heterogeneous than that of the underlying Shuba Member. It comprises oolitic dunes in the eastern sections and sandbodies that are in one case connected between the logged sections. Evaporites as well as an abundant siliciclastic component are present in the western sections (Wadis Ghalilah and Al-Ghabbah). The broad EODs are however continuous across the study area and switch to a shallow- to open marine carbonate system, containing no evidence for subaerial exposure. The western sections however contain more restricted EOD facies types (Fig. 12). The palaeogeographic map for the Early Jurassic is thus similar to previously published maps (Fig. 13C). A closer look at the EOD and facies distribution reveals heterogeneity at the scale of tens of kilometres, similar to what has been previously established for the hundreds of metre to kilometre scale in shallow-marine carbonates from Middle Jurassic strata on the Musandam Peninsula (Hönig and John, 2015).

6.5 Controls on the regional development of the platform

The overall EOD across the study area shifts from a shallow-marine carbonate system with diverse facies associations containing corals, different bioclasts and ooids to a microbialite-dominated mud- or tidalflat with abundant siliciclastic material and frequent exposure events, back to a deeper, more open-marine carbonate system, which contains only one local exposure surface. The demise of the ooid-dominated high-energy carbonate ramp, followed by an intertidal microbialite-dominated system was either induced by changes in oceanographic conditions or by a drop in relative sea level (James, 1997; Pomar and Hallock, 2008). The top of the Sakhra Member oolite at Wadi Naqab is marked by a karstified surface, which favours the model of a major relative sea level drop followed by a hiatus lasting long enough to form this karstified surface. There is however no evidence for karstification of the top Sakhra present within the other sections, despite the drastic facies and EOD change. At Wadi Ghalilah one horizon within the Sakhra Member oolite exhibits a strongly mottled surface as well as a palaeokarst. An abrupt drop in relative sea level, followed potentially by an omission phase is postulated. Restricted oceanographic conditions favouring microbialite growth, such as increased salinity (e.g. Vennin et al., 2015 and references therein) might have prevailed locally on the extensive shelf area. The Shuba Member contains bioclastic and ooidal limestones in its lower part in the western sections (Wadis Ghalilah and Al-Ghabbah), so restricted conditions could have not prevailed across the entire shelf initially, following the relative sea level drop causing the demise of the Sumra and Sakhra Member carbonate system. Environmental stress might have increased during the deposition of the Shuba Member, favouring microbialite growth.

The second switch, back to a healthy carbonate system and slightly preceding the Triassic-Jurassic boundary is the result of a relative sea level deepening, evidenced by deeper, more open-marine facies types as well as the absence of regional subaerial exposure within the Upper Shuba Member and the Musandam Limestone. It could have only been caused by either an increased subsidence rate or by a eustatic rise.

Two orders of cycles have been recognised within the studied strata. An even higher-frequency cyclicity in the Liassic of Wadi Naqab as well as the nearby Oman Mountains was previously interpreted as the result of orbital forcing (de Matos, 1997; Walkden and de Matos, 2000; Bendias and Aigner, 2015). The observed medium- and large-scale cycles also

represent changes in relative sea level, most prominently marked by various exposure stages, of which some from within the Lower Shuba Member are continuous across the entire region (Fig. 12). Although autocyclic variations might have played a role in the production of the stratigraphic pattern, they are not able to produce long lasting stages of exposure (Burgess, 2001). The inferred oscillations of relative sea level on the investigated scale were either induced by eustasy or tectonic processes. Although the eastern margin of the Arabian Plate is considered a passive margin during much of the Mesozoic (Searle, 1988; Glennie, 2005), evidence for synsedimentary extension is present within the Shuba Member (Fig. 7D). An overall extensional regime with multiple subsiding fault blocks provides an explanation for the larger accommodation available in the north western part of the study area, as evidenced by overall larger cycle thicknesses within the Wadi Al-Ghabbah section. This would have furthermore resulted in a variable palaeotopography across the shelf.

The tidal flat, the open-marine and the restricted marine EODs contain lenses of marl and shale deposits that are mostly discontinuous over the entire study area (Fig. 12). This has also been reported for the subsurface of the emirate of Abu Dhabi. The age-equivalent reservoir formations that lie in the immediate proximity in the UAE are the Minjur and Marrat Formations onshore, and the Gulailah, Hamlah and Izhara Formations offshore. The published sedimentological data on these units is still relatively scarce. Marls and shales are especially abundant within the Marrat Formation, where gamma ray peaks often cannot be correlated over more than a few tens of kilometres (Taher et al., 2012). The shale beds are especially prominent within the shallow, restricted EOD in the Lower Shuba Member (Fig. 12). Clastic material is transported from the hinterland and the interfingering marl and shale deposits are thus a function of clastic supply onto the carbonate-dominated ramp and the availability of accommodation with calm hydrodynamic conditions, especially to deposit the fine grained sediments. This clastic supply from the hinterland could be induced by increased continental runoff at times. Consequently climatically induced changes could also have played an important role in the distribution of clastic deposits on the carbonate ramp. The coarser silt- and sandstones contain evidence for both current, possibly tidal, and occasional storms crossing the shelf. It is postulated that these coarser grained and well-sorted sandbodies would have been shifted across the shelf by different hydrodynamic processes

and deposited wherever hydrodynamic and bathymetric conditions favoured deposition. The coarser material can be found in the studied sections irrespective of the interpreted relative sea level, as they are also present within the more open-marine Jurassic strata, unlike the shales and marls. A climatically induced clastic input, i.e. a switch from humid to arid conditions, would have resulted in the entire termination of clastic input. The finer clastic components during the Late Triassic and Early Jurassic were most likely transported to more distal parts of the shelf, where hydrodynamic quiescence prevailed. The Lower Jurassic deep-sea record of the Eastern Oman Mountains contains turbidite successions and silt- and sandstones, supporting the assumption of constant siliciclastic runoff (Blendinger, 1988; Blechschmidt et al., 2004).

6.6 Responses to global changes

Observing evidence for an ocean acidification event is however difficult, especially in deep time (Greene et al., 2012). The global carbon cycle perturbations, in the form of stable carbon isotope excursion around the Triassic-Jurassic boundary, have been recorded by the shallow carbonate sections of the Musandam Peninsula (Fig. 11). The overall sedimentation is mostly continuous across the Triassic-Jurassic boundary interval on the Musandam Peninsula. The Wadi Naqab section is an exception, with a local subaerial exposure surface just below the Triassic-Jurassic transition marked by a very condensed interval. Carbonate sedimentation remains largely constant across the boundary and the studied sections provide no evidence for a biocalcification crisis. A reduced carbonate content or increase in the amount of siliciclastic material, as reported from coeval continuous carbonate successions around the Triassic-Jurassic boundary in Eastern Europe (Pálfy et al., 2001; Rožič et al., 2009; Korte and Kozur, 2011) and Western Europe (e.g. Felber et al., 2015) could also not be observed on a regional scale.

The major carbonate system changes observed within the studied section are most likely caused by changes in relative sea level. The analysed sequences allow for a construction of long and a short-term relative sea level curves (Fig. 14). The constrained chronostratigraphic age allows for a comparison with other sea level curves to establish

potential eustatic controls. The Triassic-Jurassic transition broadly falls into a period of eustatic sea level rise (Fig. 2). This is also the case for the Musandam Peninsula. Eustatic changes are thus a potential mechanism to produce the vertical stratigraphic architecture. It is noteworthy that both main observations (no evidence for a biocalcification crisis and a relative sea level highstand) associated here with the Triassic-Jurassic boundary at Wadi Naqab would also be valid if the Triassic-Jurassic boundary lies at the transition between the Sumra Member and the Sakhra Member, despite a marked carbonate factory change at this transition (Fig. 6, 12).

7. Conclusions

A shallow-marine equatorial mixed, siliciclastic carbonate ramp was studied on a regional scale on the eastern Arabian Platform. Strontium isotope analysis on well-preserved oysters and brachiopods allows the placement of a Triassic-Jurassic boundary horizon, while acknowledging previous biostratigraphic studies. The studied system changes on a regional scale from an open-marine, diverse-fauna carbonate ramp, to an intertidal microbialite dominated system with abundant siliciclastic material and regional exposure stages during the Late Triassic. The Latest Triassic is marked by a revival of an open-marine, diverse-fauna carbonate ramp, which succeeds into the Early Jurassic. All sediments were deposited within the neritic part of the shallow-marine ramp. The sections thus serve as shallow-marine carbonate archive, which is regionally continuous across the Triassic-Jurassic boundary. A combination of stable carbon isotope stratigraphy and lithostratigraphy allows the regional correlation between the different study sites. The acquired carbon isotope record is furthermore correlatable to global coeval reference curves, which highlights the capability of neritic carbonate successions in the Middle East to archive global environmental changes, and merits further exploration.

The findings of the study have led us to modify the regional palaeogeographic map of the region in accordance with available subsurface data. This implies that especially the distribution of shallow-marine, clastic facies types during the Late Triassic could extend further north in the region than previously thought. The findings of this study thus might

provide information on the regional distribution of potential reservoir and/or seal facies distribution.

The observed vertical carbonate system changes on the Musandam Peninsula were most likely caused by eustatic sea level changes. Lateral heterogeneities were governed by hydrodynamic action, including occasional tropical storms, on the extensive shelf, as well as the local palaeotopography. A comparison between the constructed regional sea level curve and global eustatic sea level curves reveals that the studied system was controlled by eustatic changes, accompanied by a locally extensional tectonic regime. The ramp development across the Triassic-Jurassic transition was governed by a transgression, as observed at other Tethyan localities. No clear evidence for a biocalcification crisis marking the Triassic-Jurassic boundary, potentially induced by a global acidification event, is present regionally within the studied succession.

Acknowledgements

We acknowledge funding from Qatar Petroleum, Shell and the Qatar Science & Technology Park. Shuram Geological Consultants, Matthew Andrew and Carl Jacquemyn supported the field expeditions. Simon Davis and Anna Joy Drury assisted with stable isotope measurements. Mélanie Gretz and Bernard Lathuilière are thanked for attempting to identify corals from the Shuba Member at Wadi Ghalilah and Cristian Mircescu is thanked for the identification of calcareous algae. The study has benefited greatly from discussions with Sylvain Richoz and Florian Maurer. Reviewers Aviv Bachan and an anonymous colleague, as well as associate editor Ian Somerville are thanked for their detailed and constructive reviews.

References

Al-Husseini, M.I., 1997. Jurassic sequence stratigraphy of the western and southern Arabian Gulf. GeoArabia 2, 4, 361-382.

Alavi, M., 2004. Regional stratigraphy of the Zagros fold-thrust belt of Iran and its proforeland evolution. American Journal of Science 304, 1-20.

Alsharhan, A.S., Nairn, A., 1994. Geology and hydrocarbon habitat in the Arabian Basin: the

Mesozoic of the State of Qatar. Geologie en Mijnbouw 72, 265–265.

Al-Suwaidi, A.H., Steuber, T., Suarez, M.B., 2016. The Triassic–Jurassic boundary event from an equatorial carbonate platform (Ghalilah Formation, United Arab Emirates). Journal of the Geological Society doi:10.6084/m9.figshare.c.3277283

Amour, F., Mutti, M., Christ, N., Immenhauser, A., Benson, G.S., Agar, S.M., Tomás, S., Kabiri, L., 2013. Outcrop analog for an oolitic carbonate ramp reservoir: A scale-dependent geologic modeling approach based on stratigraphic hierarchy. American Association of Petroleum Geologists Bulletin 97, 845–871. doi:10.1306/10231212039

Bachan, A., van de Schootbrugge, B., Fiebig, J., McRoberts, C.A., Ciarapica, G., Payne, J.L., 2012. Carbon cycle dynamics following the end-Triassic mass extinction: Constraints from paired δ13C carb and δ13C org records. Geochemistry Geophysics Geosystems 13, Q09,008. doi:10.1029/2012GC004150

Barattolo, F., Bigozzi, A., 1996. Dasycladaleans and Depositional Environment of the Upper Triassic-Liassic Carbonate Platform of the Gran Sasso (Central Apennines, Italy). Facies 35, 39-54.

Bendias, D., Aigner, T., 2015. Facies, sequence stratigraphy, reservoir and seal potential of the Mafraq Formation, Sultanate of Oman: An integrated outcrop analogue study. GeoArabia 20, 3, 17-94.

Bernecker, M., 2005. Late Triassic reefs from the Northwest and South Tethys: distribution, setting, and biotic composition. Facies 51, 442–453. doi:10.1007/s10347-005-0067-4

Bernecker, M., 2007. Facies architecture of an isolated carbonate platform in the Hawasina Basin: The Late Triassic Jebel Kawr of Oman. Palaeogeography, Palaeoclimatology, Palaeoecology 252, 270–280. doi:10.1016/j.palaeo.2006.11.054

Blechschmidt, I., Dumitrica, P., Matter, A., Krystyn, L., Peters, T., 2004. Stratigraphic architecture of the northern Oman continental margin - Mesozoic Hamrat Duru Group, Hawasina complex, Oman. GeoArabia 9, 2, 1–52.

Blendinger, D.W., 1988. Permian to Jurassic deep water sediments of the eastern Oman Mountains: Their significance for the evolution of the Arabian margin of the South Tethys. Facies 19, 1–31. doi:10.1007/BF02536819

Boggs, S., Krinsley, D., 2006. Application of cathodoluminescence imaging to the study of

sedimentary rocks. Cambridge University Press, Cambridge, UK.

Burgess, P.M., 2001. Modeling carbonate sequence development without relative sea-level oscillations. Geology 29, 1127–1130.

Cohen, A.S., Coe, A.L., 2002. New geochemical evidence for the onset of volcanism in the Central Atlantic magmatic province and environmental change at the Triassic-Jurassic boundary. Geology 30, 267-270.

Cohen, K.M., Finney, S.C., Gibbard, P.L. & Fan, J.-X., 2013; updated. The ICS International Chronostratigraphic Chart. Episodes 36, 199-204.

de Matos, J.E., 1994. Upper Jurassic - Lower Cretaceous stratigraphy: the Arab Hith and Rayda Formations in Abu Dhabi. In: Simmons, M.D. (Ed.): Micropalaeontology and Hydrocarbon Exploration in the Middle East. Chapman and Hall, London, UK, 81-111.

de Matos, J.E., 1997. Stratigraphy, sedimentation and oil potential of the Lower Jurassic to Kimmeridgian of the United Arab Emirates; outcrop and subsurface compared (PhD thesis). University of Aberdeen.

de Matos, J.E., Walkden, G.M., 2000. Stratigraphy and sedimentation of the Middle Jurassic, UAE. In: Alsharhan, A.S., Scott, R.W. (Eds.), Middle East Models of Jurassic/Cretaceous Carbonate Systems, vol. 69. Society of Economic Paleontologists and Mineralogists Special Publlication, Tulsa, OK, 21-35.

Dickson, J., 1965. A modified staining technique for carbonates in thin section. Nature 4971, 587.

Di Stefano, P., Alessi, A., Gullo, M., 1996. Mesozoic and Paleogene Megabreccias in Southern Sicily: New Data on the Triassic Paleomargin of the Siculo-Tunisian Platform. Facies 43, 101-122.

Dunham, R.J., 1962. Classification of carbonate rocks according to depositional texture. In: Ham, W.E. (Ed.), Classification of Carbonate Rocks: American Association of Petroleum Geologists Memoir vol. 1, Tulsa, OK, USA, 108-121.

Embry, A.F., Klovan, J.E., 1971. A Late Devonian reef tract on Northeastern Banks Island, NWT. Canadian Petroleum Geology Bulletin 19, 730-781.

Enos, P.D.P., Samankassou, D.E., 1998. Lofer cyclothems revisited (late Triassic, northern Alps, Austria). Facies 38, 207-228. doi:10.1007/BF02537366

Felber, R., Weissert, H.J., Furrer, H., Bontognali, T.R.R., 2015. The Triassic–Jurassic boundary in the shallow-water marine carbonates from the western Northern Calcareous Alps (Austria). Swiss Journal of Geosciences 108, 213–224. doi:10.1007/s00015-015-0192-1

Fischer, A.G., 1964. The Lofer cyclothems of the Alpine Triassic. In: Merriam, D.F. (Ed.). Tidal deposits, a casebook of recent examples and fossil counterparts, Springer, New York, USA, 235-242.

Glennie K.W., Boeuf M.G.A, Huges-Clarke M.W., Moody-Stuart M., Pilaar W.F.H., Reinhardt B.M., 1974. Geology of the Oman Mountains. Royal Geology and Mining Society (Netherlands) Transactions 31.

Glennie, K.W., 2005. The Geology of the Oman Mountains e an Outline of Their Origin. Scientific Press Ltd, Beaconsfield, UK.

Golonka, J., 2007. Late Triassic and Early Jurassic palaeogeography of the world. Palaeogeography, Palaeoclimatology, Palaeoecology 244, 297–307. doi:10.1016/j.palaeo.2006.06.041

Gomez, F.J., Astini, R.A., 2015. Sedimentology and sequence stratigraphy from a mixed (carbonate–siliciclastic) rift to passive margin transition: The Early to Middle Cambrian of the Argentine Precordillera. Sedimentary Geology 316, 39–61. doi:10.1016/j.sedgeo.2014.11.003

Greene, S.E., Martindale, R.C., Ritterbush, K.A., Bottjer, D.J., Corsetti, F.A., Berelson, W.M., 2012. Earth-Science Reviews. Earth-Science Reviews 113, 72–93. doi:10.1016/j.earscirev.2012.03.009

Hallam, A., Wignall, P.B., 1999. Mass extinctions and sea-level changes. Earth-Science Reviews 48, 217–250. doi:10.1016/S0012-8252(99)00055-0

Haq, B.U., Al-Qahtani, A.M., 2005. Phanerozoic cycles of sea-level change on the Arabian Platform. GeoArabia 10, 2, 127-160.

Hassan, T.H., 1989. The Lower and Middle Jurassic in offshore Abu Dhabi: stratigraphy and hydrocarbon occurrence. Society of Petroleum Engineers Journal 18011.

Hautmann, M., Benton, M.J., Tomasovych, A., 2008. Catastrophic ocean acidification at the Triassic-Jurassic boundary. Neues Jahrbuch für Geologie und Paläontologie-

Abhandlungen 249, 119–127.

Hesselbo, S.P., McRoberts, C.A., Pálfy, J., 2007. Triassic–Jurassic boundary events: Problems, progress, possibilities. Palaeogeography, Palaeoclimatology, Palaeoecology 244, 1–10. doi:10.1016/j.palaeo.2006.06.020

Hesselbo, S.P., Robinson, S.A., Surlyk, F., Piasecki, S., 2002. Terrestrial and marine extinction at the Triassic-Jurassic boundary synchronized with major carbon-cycle perturbation: A link to initiation of massive volcanism? Geology 30, 251–254. doi:10.1130/0091-7613(2002)030<0251:TAMEAT>2.0.CO;2

Hönig, M.R., John, C.M., 2015. Sedimentological and isotopic heterogeneities within a Jurassic carbonate ramp (UAE) and implications for reservoirs in the Middle East. Marine and Petroleum Geology 68, 240–257. doi:10.1016/j.marpetgeo.2015.08.029

Hönisch, B., Ridgwell, A., Schmidt, D.N., Thomas, E., Gibbs, S.J., Sluijs, A., Zeebe, R., Kump, L., Martindale, R.C., Greene, S.E., Kiessling, W., Ries, J., Zachos, J.C., Royer, D.L., Barker, S., Marchitto, T.M., Moyer, R., Pelejero, C., Ziveri, P., Foster, G.L., Williams, B., 2012. The Geological Record of Ocean Acidification. Science 335, 1058–1063. doi:10.1126/science.1208277

Hudson, R.G.S., 1960. The Permian and Trias of the Oman Peninsula, Arabia. Geological Magazine 97, 199-208.

Hudson R.G.S., Jefferies R.P.S., 1961. Upper Triassic brachiopods and lamellibranchs from the Oman Peninsula, Arabia. Palaeontology 4, 1–41.

Ikeda, M., Hori, R.S., Okada, Y., Nakada, R., 2015. Volcanism and deep-ocean acidification across the end-Triassic extinction event. Palaeogeography, Palaeoclimatology, Palaeoecology 440, 725–733.

Immenhauser,A., Hillgärtner,H., Sattler,U., Bertotti,G., VanderKooij,B., Van Bentum, E., Van Koppen, J., Verwer, K., Immenhauser-Potthast, I., Schoepfer, P., Vahrenkamp, V., Hoogerduijn-Strating, E., Peters, J., Homewood, P., Droste, H.J., Swinkels, W., Steuber, T., Masse, J.P., Al Maskery, S.A.J., 2004. Barremian-lower Aptian Qishn Formation, Haushi-Huqf area, Oman: a new outcrop analogue for the Kharaib/Shu'aiba reservoirs. GeoArabia 9, 1, 11-52.

James, N.P., 1997. The cool water carbonate depositional realm. In: James, N.P. and Clar-

ke, J.A.D. (Eds.). Cool-Water Carbonates. Special Publication, Society of Economic Paleontologists and Mineralogists, Tulsa, OK, USA, 56, 1-20.

John, C.M., Bowen, D., 2016. Community software for challenging isotope analysis: First applications of 'Eastope' to clumped isotopes. Rapid Communications in Mass Spectrometry 30, 2285-2300, doi:10.1002/rcm.7720.

Korte, C., Kozur, H.W., 2011. Bio-and chemostratigraphic assessment of carbon isotope records across the Triassic–Jurassic boundary at Csővár quarry (Hungary) and Kendlbachgraben (Austria) and implications for global correlations. Bulletin of the Geological Society of Denmark 59, 101-115.

Le Nindre, Y.-M., Vaslet, D., Le Métour, J., Bertrand, J., Halawani, M., 2003. Subsidence modelling of the Arabian Platform from Permian to Paleogene outcrops. Sedimentary Geology 156, 263–285.

Loufti, G., Sattar, M.M.A., 1987. Geology and Hydrocarbon Potential of the Triassic Succession in Abu Dhabi, U.A.E. Society of Petroleum Engineers Journal 15698.

Marzoli, A., Bertrand, H., Knight, K.B., Cirilli, S., Buratti, N., Vérati, C., Nomade, S., Renne, P.R., Youbi, N., Martini, R., Allenbach, K., Neuwerth, R., Rapaille, C., Zaninetti, L., Bellieni, G., 2004. Synchrony of the Central Atlantic magmatic province and the Triassic-Jurassic boundary climatic and biotic crisis. Geology 32, 973. doi:10.1130/G20652.1

Maurer, F., Krystyn, L., Martini, R., McRoberts, C., Rettori, R., Hofmann, P., 2015. Towards a Refined Arabian Plate Triassic Stratigraphy: Insights from the Musandam Peninsula (UAE and Oman). 5th EAGE Arabian Plate Geology Workshop Kuwait, Abstract P05.

Maurer, F., Martini, R., Rettori, R., Hillgärtner, H., Cirilli, S., 2009. The geology of the Khuff outcrop analogies in the Musandam Peninsula, United Arab Emirates and Oman. GeoArabia 14, 3, 125-158.

Maurer, F., Rettori, R., Martini, R., 2008. Triassic stratigraphy, facies and evolution of the Arabian shelf in the northern United Arab Emirates. International Journal of Earth Sciences (Geologische Rundschau) 97, 765–784. doi:10.1007/s00531-007-0194-y

McArthur, J.M., Howarth, R.J., Bailey, T.R., 2001. Strontium isotope stratigraphy: LOWESS version 3: Best fit to the marine Sr‐isotope curve for 0–509 Ma and accompanying look‐up table for deriving numerical age. The Journal of Geology 109, 155–170.

Meister, C., Dommergues, J.L., Rocha, R.B., 2012. Ammonites from the Apoderoceras beds (Early Pliensbachian) in São Pedro de Muel (Lusitanian Basin, Portugal). Bulletin of Geosciences 87, 407–430. doi:10.3140/bull.geosci.1325

Metwally, M.H.M., Ali, M.S.M., 1992. The Triassic-Jurassic Boundary in the Elphinstone Group, western part of the Musandam Peninsula, UAE. Neues Jahrbuch für Geologie und Paläontologie Mh. 5, 257-266.

Miller, K.G., Kominz, M.A., Browning, J.V., Wright, J.D., Mountain, G.S., Katz, M.E., Sugarman, P.J., Cramer, B.J., Christie-Blick, N., Pekar, S.F., 2005. The Phanerozoic Record of Global Sea-Level Change. Science 310, 1293–1298. doi:10.1126/science.1116412

Pálfy, J., Demény, A., Haas, J., Hetényi, M., Orchard, M.J., Veto, I., 2001. Carbon isotope anomaly and other geochemical changes at the Triassic-Jurassic boundary from a marine section in Hungary. Geology 29, 1047–1050. doi:10.1130/0091-7613(2001)029<1047:CIAAOG>2.0.CO;2

Pierre, A., 2006. Un analogue de terrain pour les rampes oolitiques anciennes. Un affleurement continu à l'eéchelle de la sismique (falaises jurassiques d'Amellago, Haut Atlas, Maroc) (PhD Thesis). Université de Bourgogne.

Pomar, L., Hallock, P., 2008. Carbonate factories: A conundrum in sedimentary geology. Earth-Science Reviews 87, 134–169. doi:10.1016/j.earscirev.2007.12.002

Rousseau, M., Dromart, G., Garcia, J.P., Atrops, F., Guillocheau, F., 2005. Jurassic evolution of the Arabian carbonate platform edge in the central Oman Mountains. Journal of the Geological Society 162, 349–362. doi:10.1144/0016-764903-178

Rožič, B., Kolar-Jurkovšek, T., Šmuc, A., 2009. Late Triassic sedimentary evolution of Slovenian Basin (eastern Southern Alps): description and correlation of the Slatnik Formation. Facies 55, 137–155.

Searle, M.P., 1988. Thrust tectonics of the Dibba zone and the structural evolution of the Arabian continental margin along the Musandam mountains (Oman and United Arab Emirates). Journal of the Geological Society 145, 43–53. doi:10.1144/gsjgs.145.1.0043

Satterley, A.K., Brandner, R., 1995. The genesis of Lofer cycles of the Dachstein Limestone, Northern Calcareous Alps, Austria. Geologische Rundschau 84, 287-292.

Searle, M.P., Cherry, A.G., Ali, M.Y., Cooper, D., 2014. Tectonics of the Musandam Peninsula and northern Oman Mountains: From ophiolite obduction to continental collision. GeoArabia 19, 2, 135-174.

Sharland, P.R., Archer, R., Casey, D.M., Davies, R.B., Hall, S.H., Heward, A.P., Horbury, A.D., Simmons, M.D., 2001. Arabian Plate Sequence Stratigraphy. Gulf PetroLink, Manama, Bahrain.

Strasser, A., Pittet, B., Hillgärtner, H., Pasquier, J.-B., 1999. Depositional sequences in shallow carbonate-dominated sedimentary systems: concepts for a high-resolution analysis. Sedimentary Geology 128, 201–221.

Taher, A., Al Shateri, A., Al Mehsin, K., Witte, J., Al Zaabi, M., Obaid, K., 2012. Tight Gas Exploration Potential of Middle Triassic to Early Jurassic Successions in Abu Dhabi. Society of Petroleum Engineers Journal 162355.

Tanner, L.H., Lucas, S.G., Chapman, M.G., 2004. Assessing the record and causes of Late Triassic extinctions. Earth-Science Reviews 65, 103–139. doi:10.1016/S0012-8252(03)00082-5

Thierry, J., Barrier, E., 2000. Middle Toarcian. In: Dercourt, J., Gaetani, M., Vrielynck, B., Barrier, E., Biju-Duval, B., Brunet, M.F., Cadet, J.-P., Crasquin, S., Sandulescu, M. (Eds.), Atlas Peri-tethys, Palaeogeographical Maps (Commission de la carte géologique du monde: Paris).

Thirlwall, M.F., 1991. Long-term reproducibility of multicollector Sr and Nd isotope ratio analysis: Chemical Geology: Isotope Geoscience Section 94, 85–104.

Vennin, E., Olivier, N., Brayard, A., Bour, I., Thomazo, C., Escarguel, G., Fara, E., Bylund, K.G., Jenks, J.F., Stephen, D.A., Hofmann, R., 2015. Microbial deposits in the aftermath of the end-Permian mass extinction: A diverging case from the Mineral Mountains (Utah, USA). Sedimentology 62, 3, 753-792. doi:10.1111/sed.12166

Walkden, G.M., de Matos, J.E., 2000. “Tuning” High-Frequency Cyclic Carbonate Platform Successions using Omission Surfaces: Lower Jurassic of the UAE and Oman. In: Alsharhan, A.S., Scott, R.W. (Eds.), Middle East Models of Jurassic/ Cretaceous Carbonate Systems, vol. 69. Society of Economic Paleontologists and Mineralogists Special Publication, Tulsa, OK, pp. 37-52.

Warren, J.K., Kendall, C.G.St.C., 1985. Comparison of Sequences Fromed in Marine Sabkha (Subaerial) and Salina (Subaqueous) Settings – Modern and Ancient. American Association of Petroleum Geologists Bulletin 69, 1013-1023.

Williford, K.H., Ward, P.D., Garrison, G.H., Buick, R., 2007. An extended organic carbon-isotope record across the Triassic–Jurassic boundary in the Queen Charlotte Islands, British Columbia, Canada. Palaeogeography, Palaeoclimatology, Palaeoecology 244, 290–296. doi:10.1016/j.palaeo.2006.06.032

Ziegler, M.A., 2001. Late Permian to Holocene paleofacies evolution of the Arabian Plate and its hydrocarbon occurrences. GeoArabia 6, 3, 445-504.

Figure captions

Fig. 1 - **A)** Location map of the study area. **B)** Palaeogeographic setting of the Tethyan realm during the Early Jurassic (modified from Pierre, 2006; after Thierry and Barrier, 2000).

Fig. 2 - Late Triassic – Early Jurassic chronostratigraphy and different biostratigraphic frameworks from the Musandam Peninsula combined with chemostratigraphic data (strontium and carbon isotopes) and different sea-level curves. The red font indicates taxa identified as part of this study.

Fig. 3 - **A)** Panoramic view of the studied formations in Wadi Naqab. **B)** Abundant vugs within a brown dolo-mudstone bed. **C)** White calcite cement nodule with pink dolomite cement in the centre (both from within the Shuba Member at Wadi Al-Ghabbah) **D)** Whitish microbial laminite overlain by fenestral limestone (from the Shuba Member at Wadi Naqab). **E, F)** Dasycladalean algae *Paleodasycladus* sp. (from the Upper Shuba Member at Wadi Naqab; pen is 14.5 cm long).

Fig. 4 - **A)** Tepee structure within a microbial laminite bed (from the Shuba Member at Wadi Naqab). **B)** Channelized bioclastic wackestone (from the Shuba Member at Wadi Ghalilah;

hammer is 28 cm long). **C)** Stained thin section image of an ooidal grainstone. **D)** Thin section image of a bioclastic grainstone. **E)** Detailed panorama of the oolitic, cross-stratified dune at the base of the Musandam Limestone, including a rose diagram of the palaeocurrent measurements. **F)** Detailed view of the oolitic dune shown in E. Black lines indicate bedding planes. Red lines indicate cross beds. **G)** Detailed view of at the contact between a bedding plane and a cross bed with a mudstringer in between (all from Wadi Naqab).

Fig. 5 - **A)** Branching coral in living position from the Shuba Member in Wadi Ghalilah. **B)** Stained thin section image of calcite-cemented quartz sandstone. **C)** Large coral head, top Sumra Member at Wadi Naqab. **D)** Branching corals from the top Sumra Member at Wadi Naqab. **E)** Well-preserved coral fragments (from the top Sumra Member at Jabal Sall Ala (all corals *Retiophyllia* (?), sensu Maurer et al., 2008). **F)** Cross-laminated sandstone from the top of the Shuba Member at Wadi Al-Ghabbah. **G)** Lenticular bedding in a sandstone bed at the top of the Shuba Member at Wadi Al-Ghabbah. **H)** Hummocky cross-stratification in a sandstone bed at the top of the Shuba Member at Wadi Al-Ghabbah. **I)** Monomictic conglomerate from the Shuba Member in Wadi Ghalilah (pen is 14.5 cm long).

Fig. 6 - Detailed sedimentological sections from the four study sites, including stable carbon isotope curves. The chronostratigraphic boundaries for the Wadi Naqab section are placed in accordance with strontium isotope results obtained in this study and biostratigraphic markers (positions of samples used for Sr isotope analysis are indicated on the Wadi Naqab log; [1] from Maurer et al., 2008; [2] from de Matos, 1997; [2]* from de Matos, 1997 - observed in Wadi Milaha; m: marl; M: mudstone; W: wackestone; P: packstone; G: grainstone; F: floatstone; R: rudstone; B: boundstone).

Fig. 7 - **A)** Karstified and stained top of the Sakhra Member oolite, Wadi Naqab. **B)** Desiccation cracks on a bedding surface from the Shuba Member in Wadi Ghalilah. **C)** Karst infill within the Sakhra Member oolite at Wadi Ghalilah. **D)** Synsedimentary normal fault within a fenestral mudstone bed of the Shuba Member in Wadi Ghalilah (hammer is 28 cm long).

Fig. 8 - Crossplot between all $\delta^{18}O$ and $\delta^{13}C$ measurements from the three measured sections.

Fig. 9 - **A)** Thin section image of a brachiopod from sample WN 193. **B)** Cathodoluminescence image of A. **C)** Thin section image of an oyster from sample WN 168 Oy. **D)** Cathodoluminescence image of C. **E)** Thin section image of an oyster from sample WN TJ B. F) Cathodoluminescence image of E. The scale bar in all images is 500 µm long.

Fig. 10 - **A)** Detailed sample positions selected for Sr isotope analysis from the Wadi Naqab section (see Fig. 4.6 for the facies colour code and Dunham texture abbreviations). **B)** Measured $^{87}Sr/^{86}Sr$ data (left side of the plot) used for numerical age determination via the Late Triassic to Early Jurassic part of the LOWESS best-fit curve (McArthur et al., 2001). Values from the LOWESS best-fit curve within the 95 % confidence level are shown.

Fig. 11 - Comparison of selected $\delta^{13}C$ reference curves compared to the composite $\delta^{13}C$ curve from the Musandam Peninsula. Potential correlation patterns are marked with coloured arrows and lines. A lithological control on the $\delta^{13}C$ signal of section measured on the Musandam Peninsula cannot be fully excluded. The “initial” and “main” carbon isotope excursions (Hesselbo et al., 2002) are indicated (A: Williford et al., 2007; B: Bachan et al., 2012; C: Hesselbo et al., 2002).

Fig. 12 - South to North correlations between environments of deposition across the Musandam Peninsula between the studied sections, based on chemo- and lithostratigraphic correlations. Medium- and large-scale sequences are indicated (see Fig. 4.6 for the Dunham texture abbreviations).

Fig. 13 - **A)** Palaeogeographic map of the Arabian Peninsula for the Late Triassic - Early Jurassic interval. **B)** Detailed and refined palaeogeographic map of the north-eastern Arabian Peninsula, incorporating published well data from Abu Dhabi during the Late Triassic. **C)** Detailed and refined palaeogeography during the Early Jurassic.

Fig. 14 - Chronostratigraphic framework from the Musandam Peninsula with a relative sea level curve, based on the interpreted accommodation space changes.

Table 1 - Description, dimensions and interpretation of the nine observed lithofacies associations (LF); (m: marl; M: mudstone; W: wackestone; P: packstone; G: grainstone; F: floatstone; R: rudstone; B: boundstone).

Appendices (separate Excel file)

- C and O isotope raw data

- Sr raw data

Figure 1

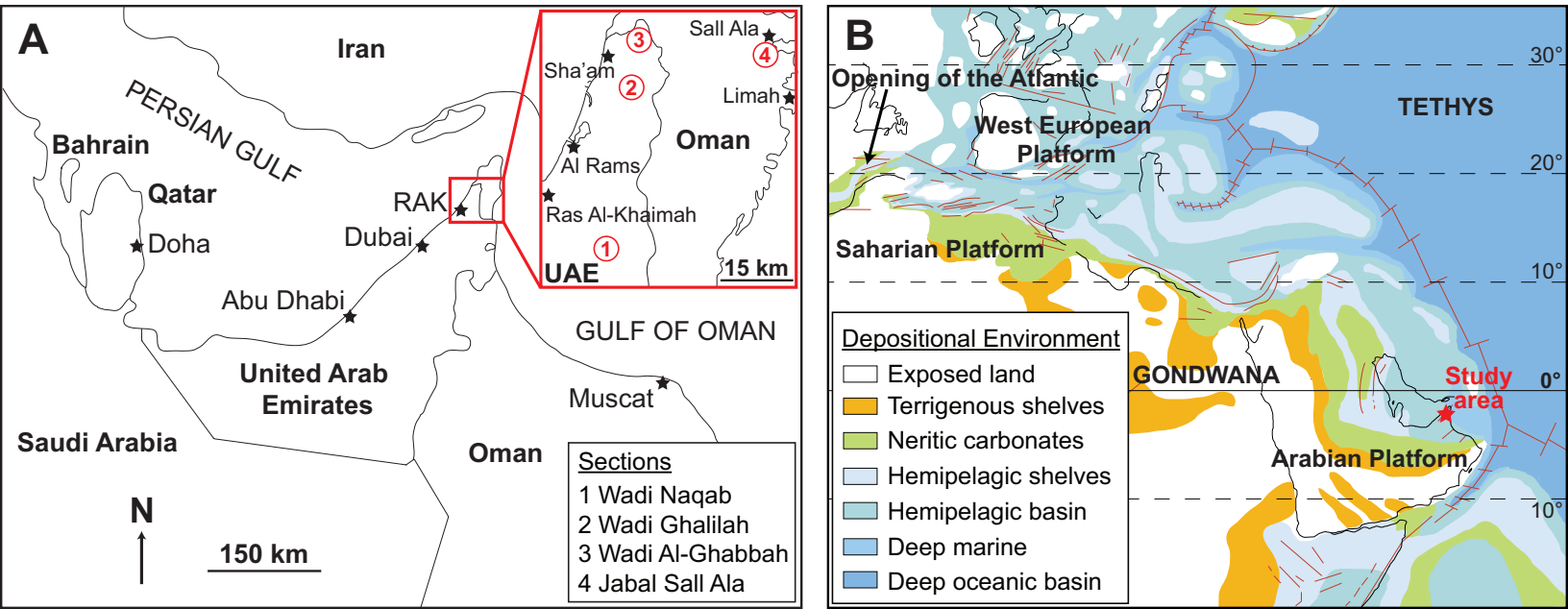
A
Iran
PERSIAN GULF
Bahrain
Qatar
Doha
RAK
Dubai
Abu Dhabi
United Arab Emirates
Saudi Arabia
Oman
GULF OF OMAN
Muscat
N
150 km
Sall Ala
Sha'am
Limah
Oman
Al Rams
Ras Al-Khaimah
UAE
15 km
Sections
1 Wadi Naqab
2 Wadi Ghalilah
3 Wadi Al-Ghabbah
4 Jabal Sall Ala
B
Opening of the Atlantic
West European Platform
TETHYS
Saharian Platform
GONDWANA
Study area
Arabian Platform
30°
20°
10°
0°
10°
Depositional Environment
Exposed land
Terrigenous shelves
Neritic carbonates
Hemipelagic shelves
Hemipelagic basin
Deep marine
Deep oceanic basin

Figure 2

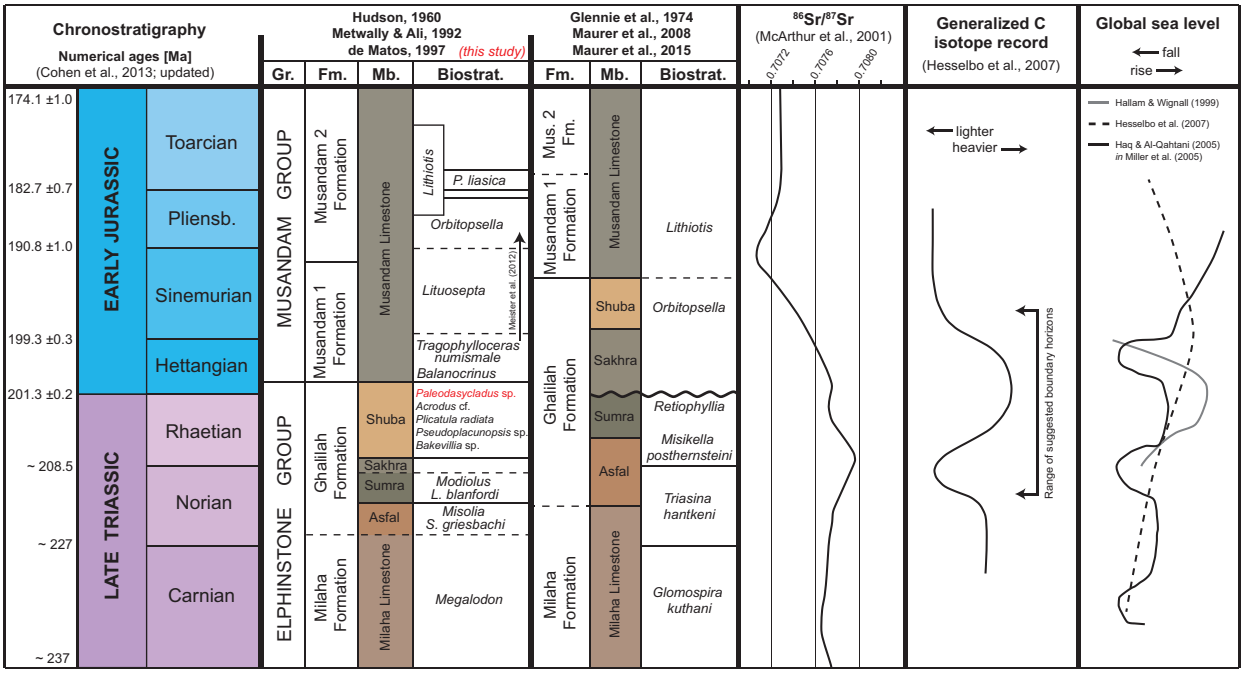
Chronostratigraphy
Numerical ages [Ma]
(Cohen et al., 2013; updated)
174.1 ±1.0
182.7 ±0.7
190.8 ±1.0
199.3 ±0.3
201.3 ±0.2
~ 208.5
~ 227
~ 237
EARLY JURASSIC
LATE TRIASSIC
Toarcian
Pliensb.
Sinemurian
Hettangian
Rhaetian
Norian
Carnian
Hudson, 1960
Metwally & Ali, 1992
de Matos, 1997 (this study)
Gr.
Fm.
Mb.
Biostrat.
MUSANDAM GROUP
ELPHINSTONE GROUP
Musandam 2 Formation
Musandam 1 Formation
Ghalilah Formation
Milaha Formation
Musandam Limestone
Shuba
Sakhra
Sumra
Asfal
Milaha Limestone
Lithiotis
P. liasica
Orbitopsella
Lituosepta
Tragophylloceras numismale
Balanocrinus
Paleodasycladus sp.
Acrodus cf.
Plicatula radiata
Pseudoplacunopsis sp.
Bakevillia sp.
Modiolus
L. blanfordi
Misolia
S. griesbachi
Megalodon
Meister et al. (2012)
Glennie et al., 1974
Maurer et al., 2008
Maurer et al., 2015
Fm.
Mb.
Biostrat.
Mus. 2 Fm.
Musandam 1 Formation
Ghalilah Formation
Milaha Formation
Musandam Limestone
Shuba
Sakhra
Sumra
Asfal
Milaha Limestone
Lithiotis
Orbitopsella
Retiophyllia
Misikella posthernsteini
Triasina hantkeni
Glomospira kuthani
86Sr/87Sr
(McArthur et al., 2001)
0.7072
0.7076
0.7080
Generalized C isotope record
(Hesselbo et al., 2007)
lighter
heavier
Range of suggested boundary horizons
Global sea level
fall
rise
Hallam & Wignall (1999)
Hesselbo et al. (2007)
Haq & Al-Qahtani (2005)
in Miller et al. (2005)

Figure 3

Click here to download high resolution image

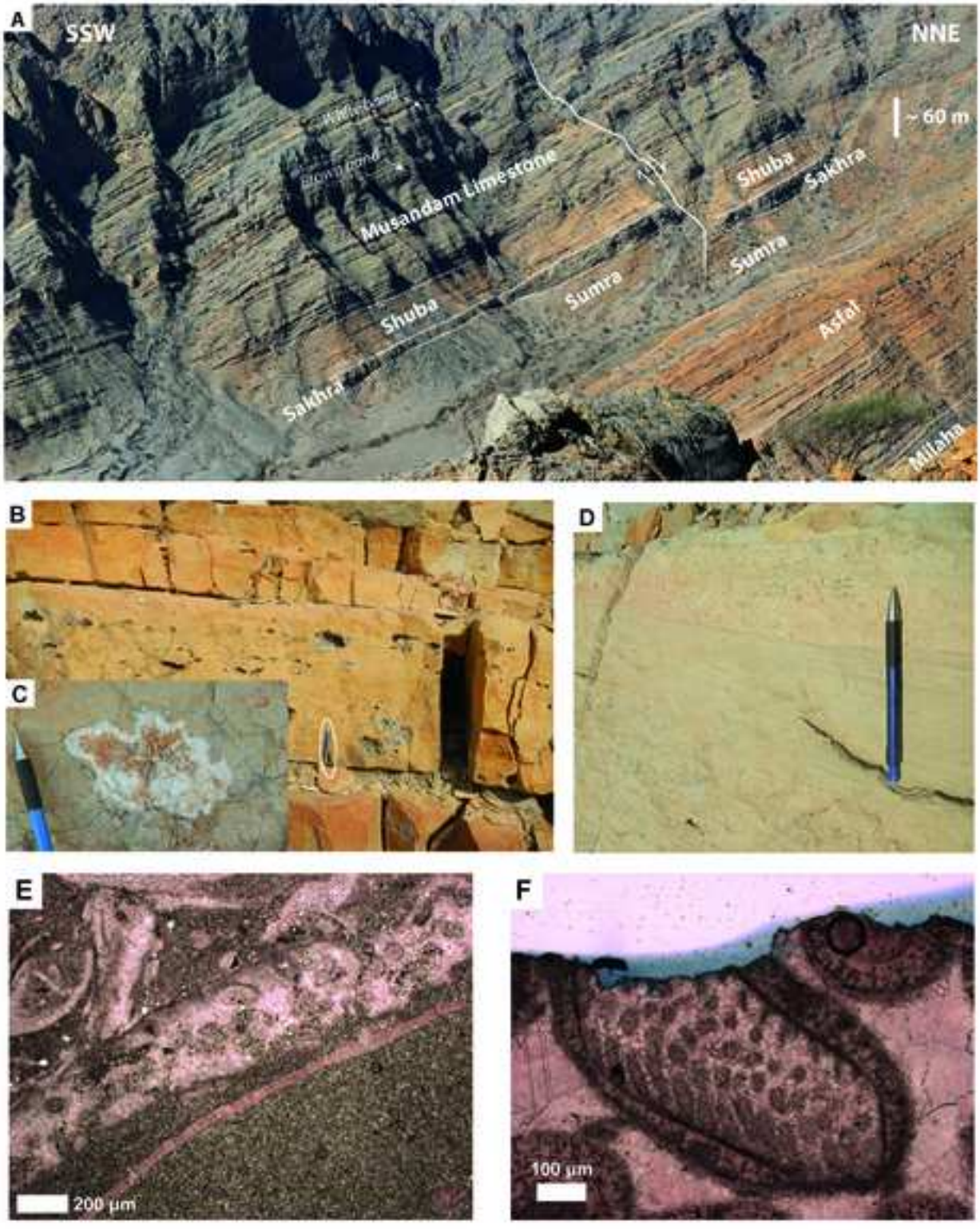

Figure 4

Click here to download high resolution image

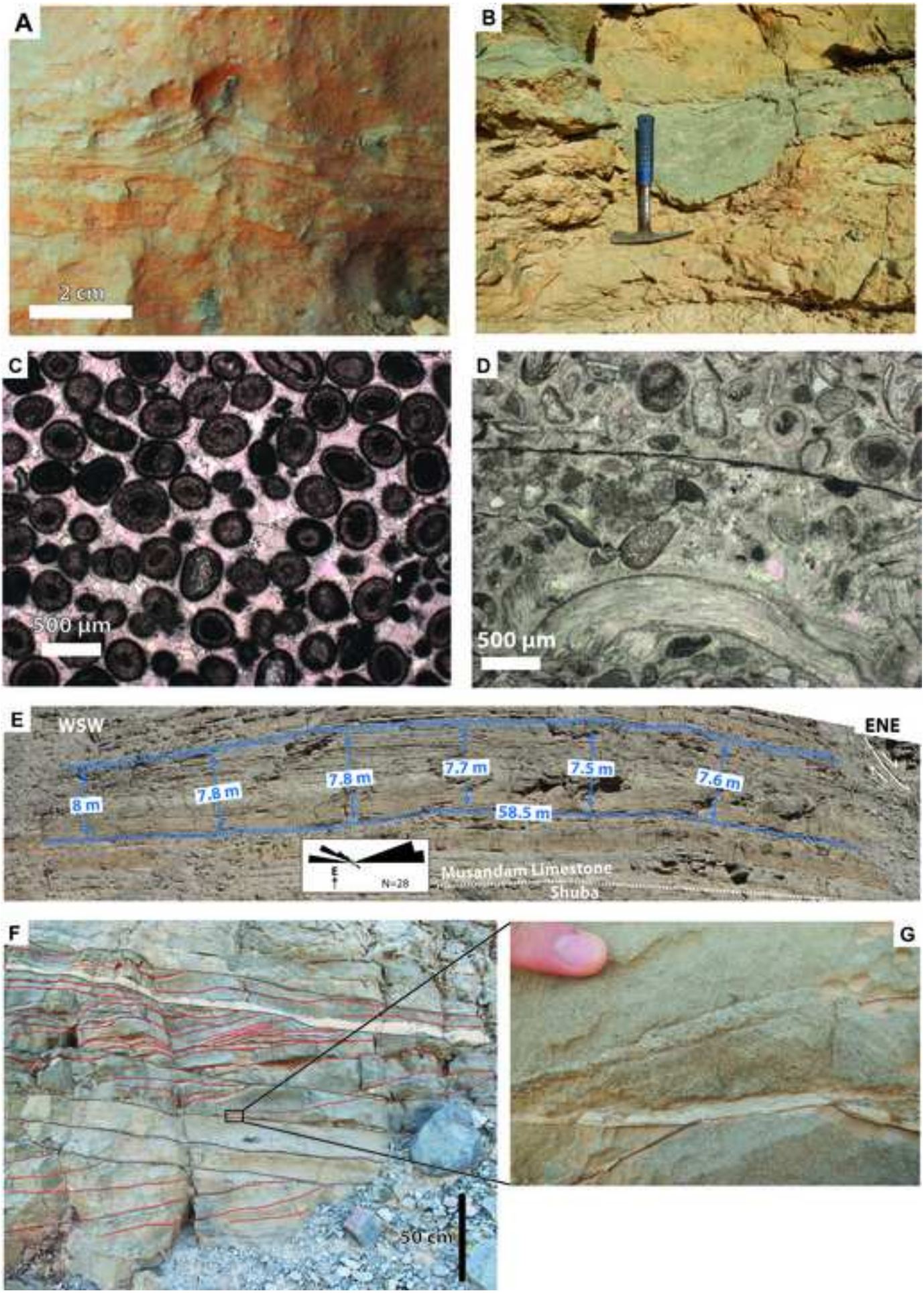

Figure 5

Click here to download high resolution image

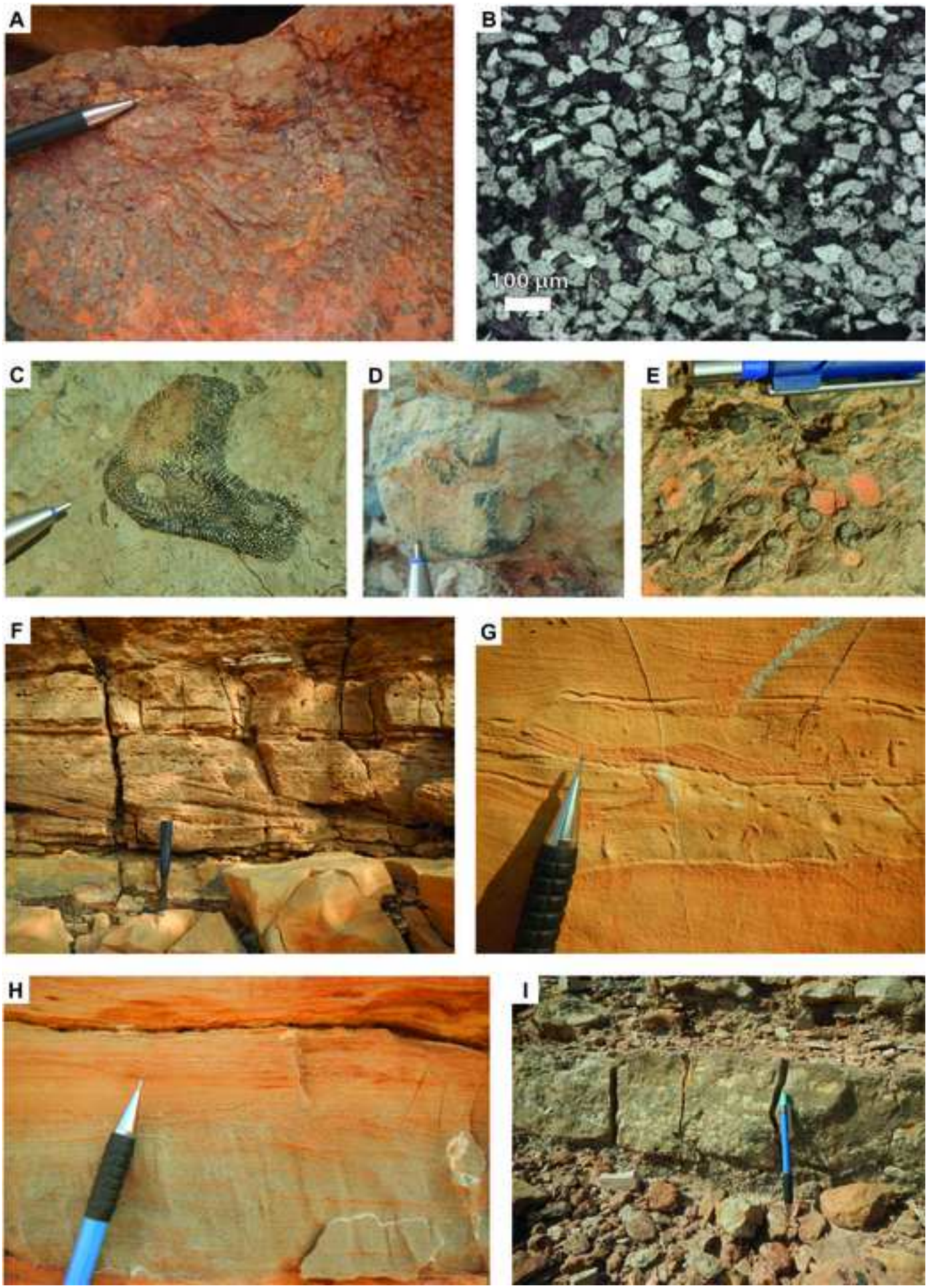

Figure 6

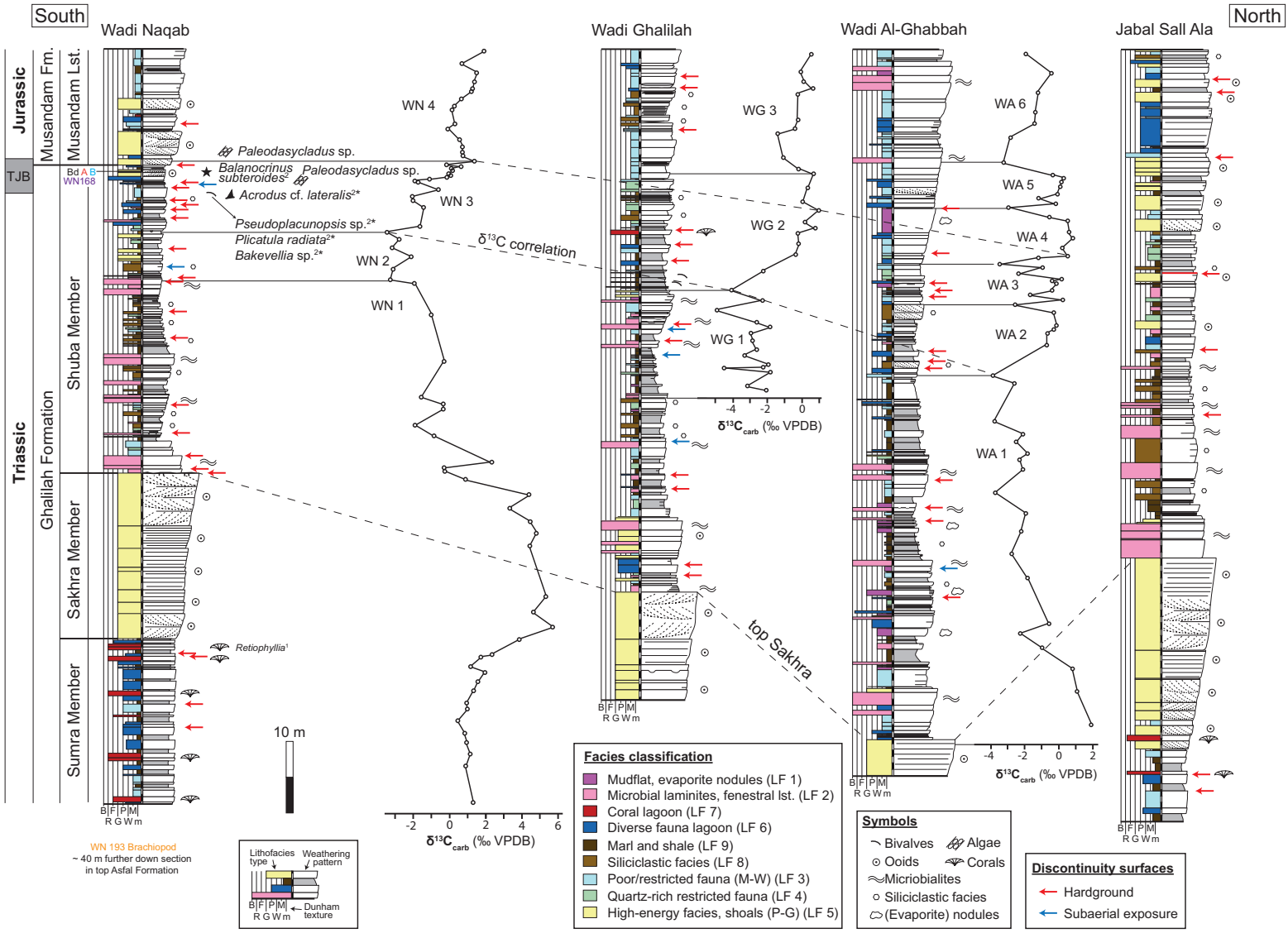
South
North
Wadi Naqab
Wadi Ghalilah
Wadi Al-Ghabbah
Jabal Sall Ala
Jurassic
Triassic
TJB
Musandam Fm.
Musandam Lst.
Ghalilah Formation
Shuba Member
Sakhra Member
Sumra Member
Bd A B
WN168
Paleodasycladus sp.
Balanocrinus subteroides²
Paleodasycladus sp.
Acrodus cf. lateralis²*
Pseudoplacunopsis sp.²*
Plicatula radiata²*
Bakevellia sp.²*
Retiophyllia¹
WN 4
WN 3
WN 2
WN 1
δ¹³C correlation
top Sakhra
WG 3
WG 2
WG 1
WA 6
WA 5
WA 4
WA 3
WA 2
WA 1
δ¹³C_carb (‰ VPDB)
B F P M
R G W m
10 m
WN 193 Brachiopod
~ 40 m further down section
in top Asfal Formation
Lithofacies type
Weathering pattern
Dunham texture
Facies classification
Mudflat, evaporite nodules (LF 1)
Microbial laminites, fenestral lst. (LF 2)
Coral lagoon (LF 7)
Diverse fauna lagoon (LF 6)
Marl and shale (LF 9)
Siliciclastic facies (LF 8)
Poor/restricted fauna (M-W) (LF 3)
Quartz-rich restricted fauna (LF 4)
High-energy facies, shoals (P-G) (LF 5)
Symbols
Bivalves
Algae
Ooids
Corals
Miciobialites
Siliciclastic facies
(Evaporite) nodules
Discontinuity surfaces
Hardground
Subaerial exposure

Figure 7

Click here to download high resolution image

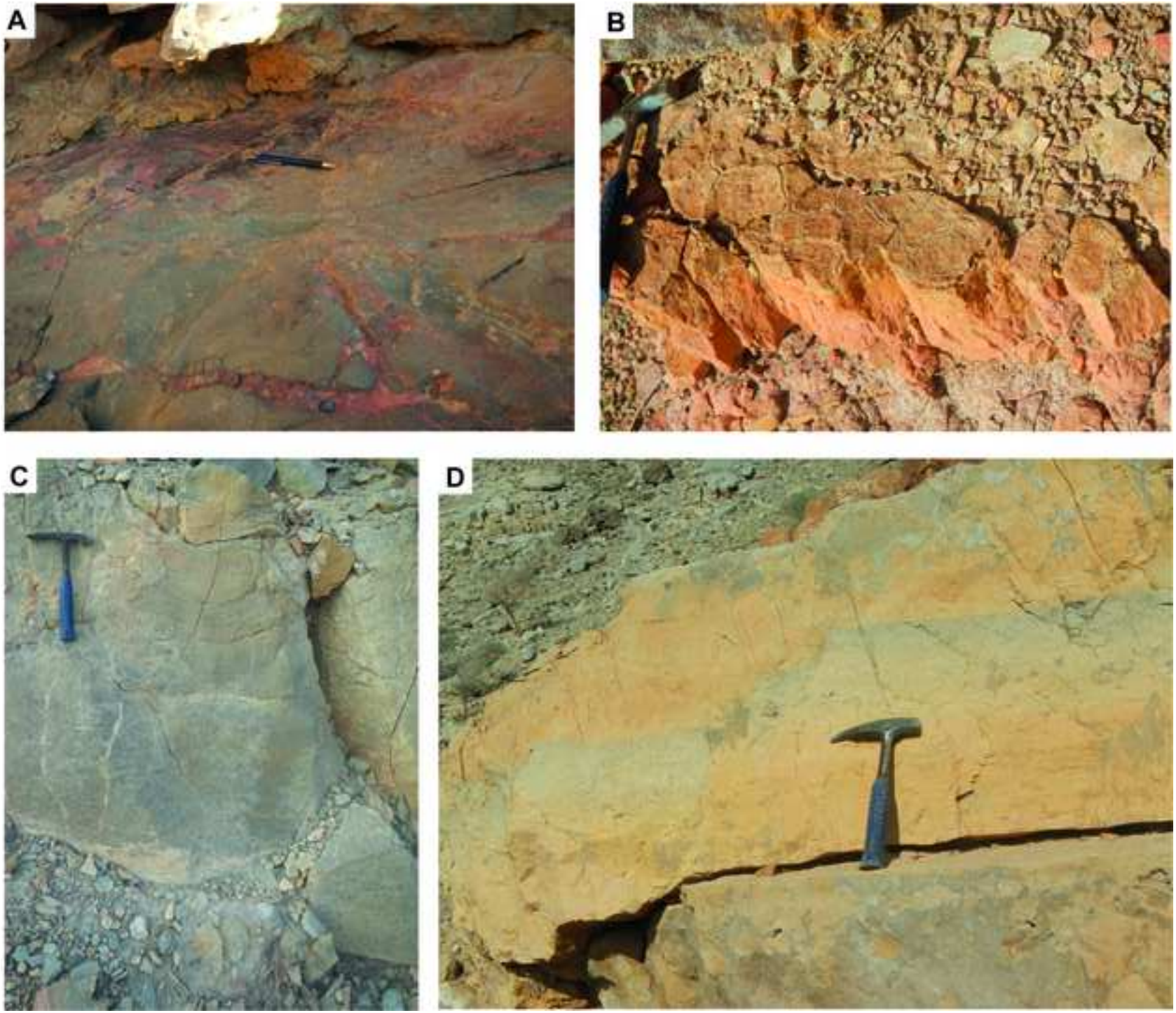

Figure 8

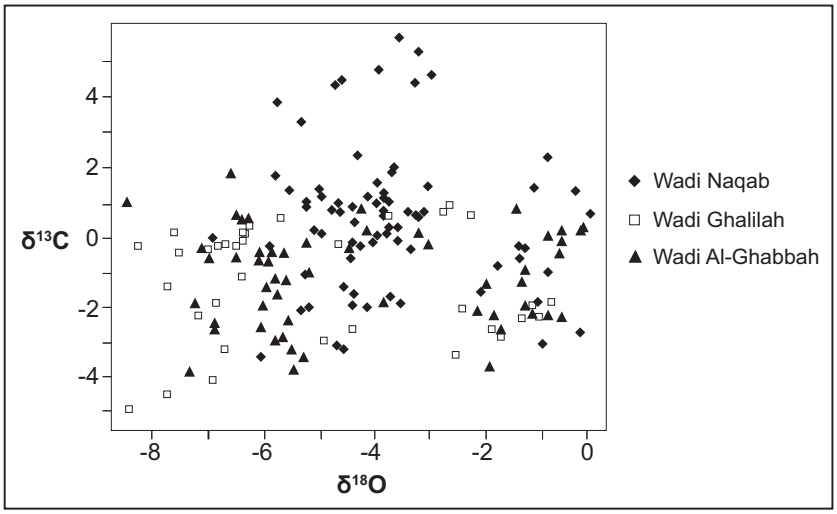
δ13C
4
2
0
-2
-4
-8
-6
-4
-2
0
δ18O
Wadi Naqab
Wadi Ghalilah
Wadi Al-Ghabbah

Figure 9

Click here to download high resolution image

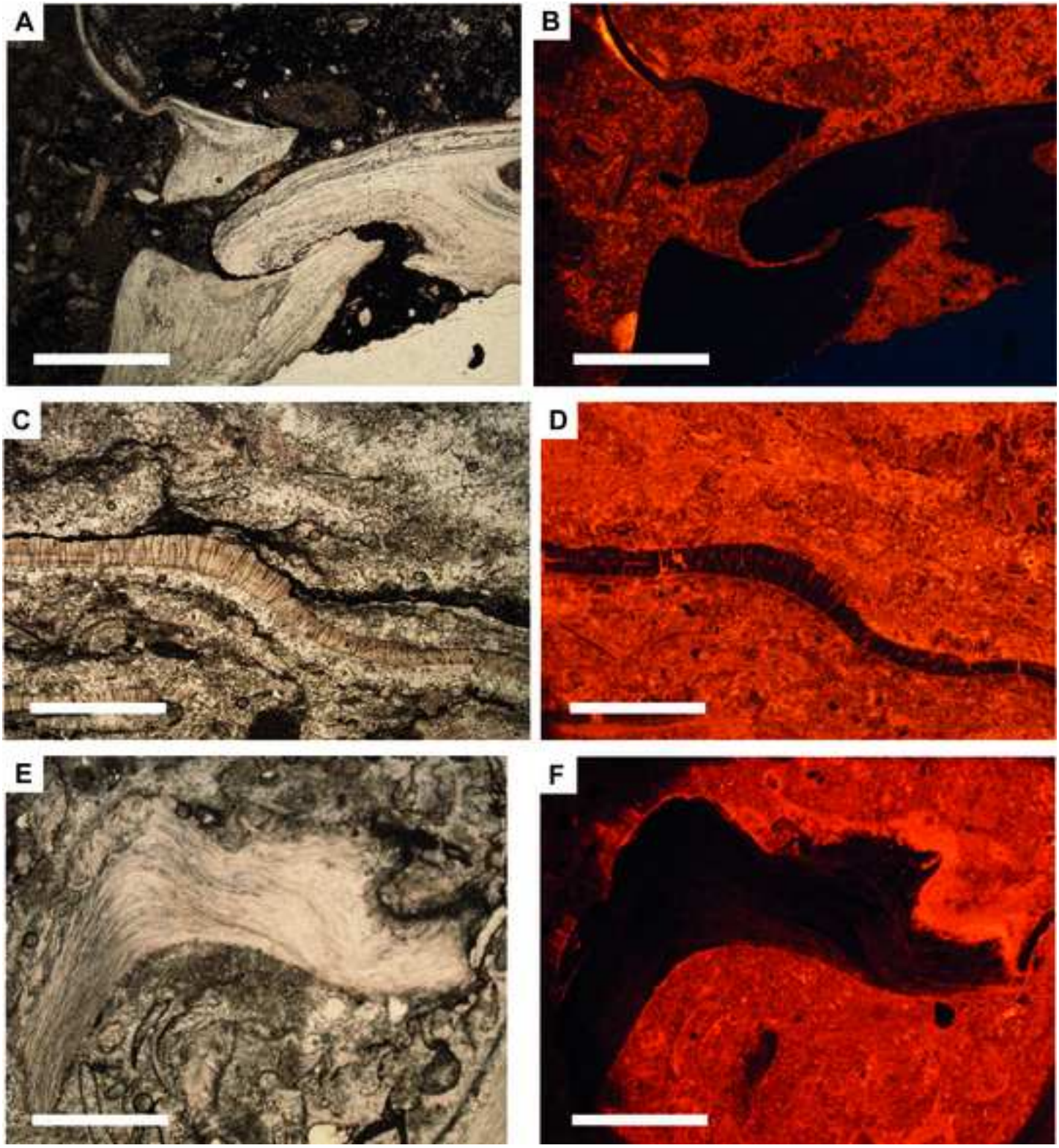

Figure 10

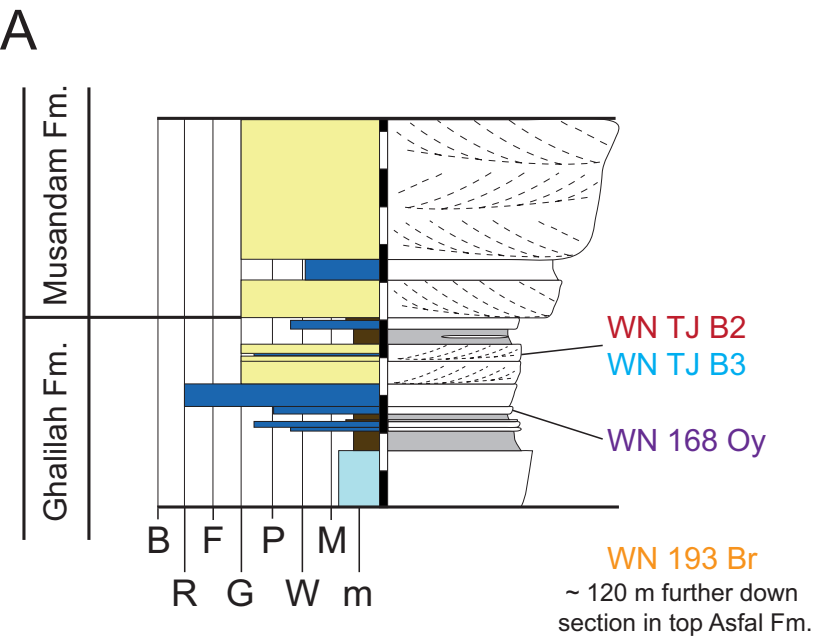
A
Musandam Fm.
Ghalilah Fm.
B F P M
R G W m
WN TJ B2
WN TJ B3
WN 168 Oy
WN 193 Br
~ 120 m further down
section in top Asfal Fm.

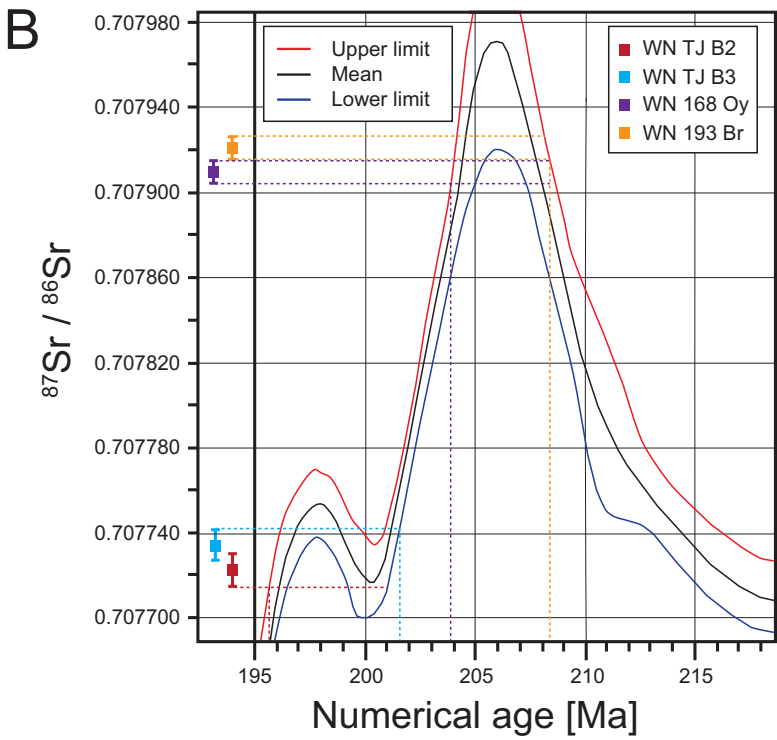
B
Upper limit
Mean
Lower limit
WN TJ B2
WN TJ B3
WN 168 Oy
WN 193 Br
0.707980
0.707940
0.707900
0.707860
0.707820
0.707780
0.707740
0.707700
87Sr / 86Sr
195
200
205
210
215
Numerical age [Ma]

Figure 11

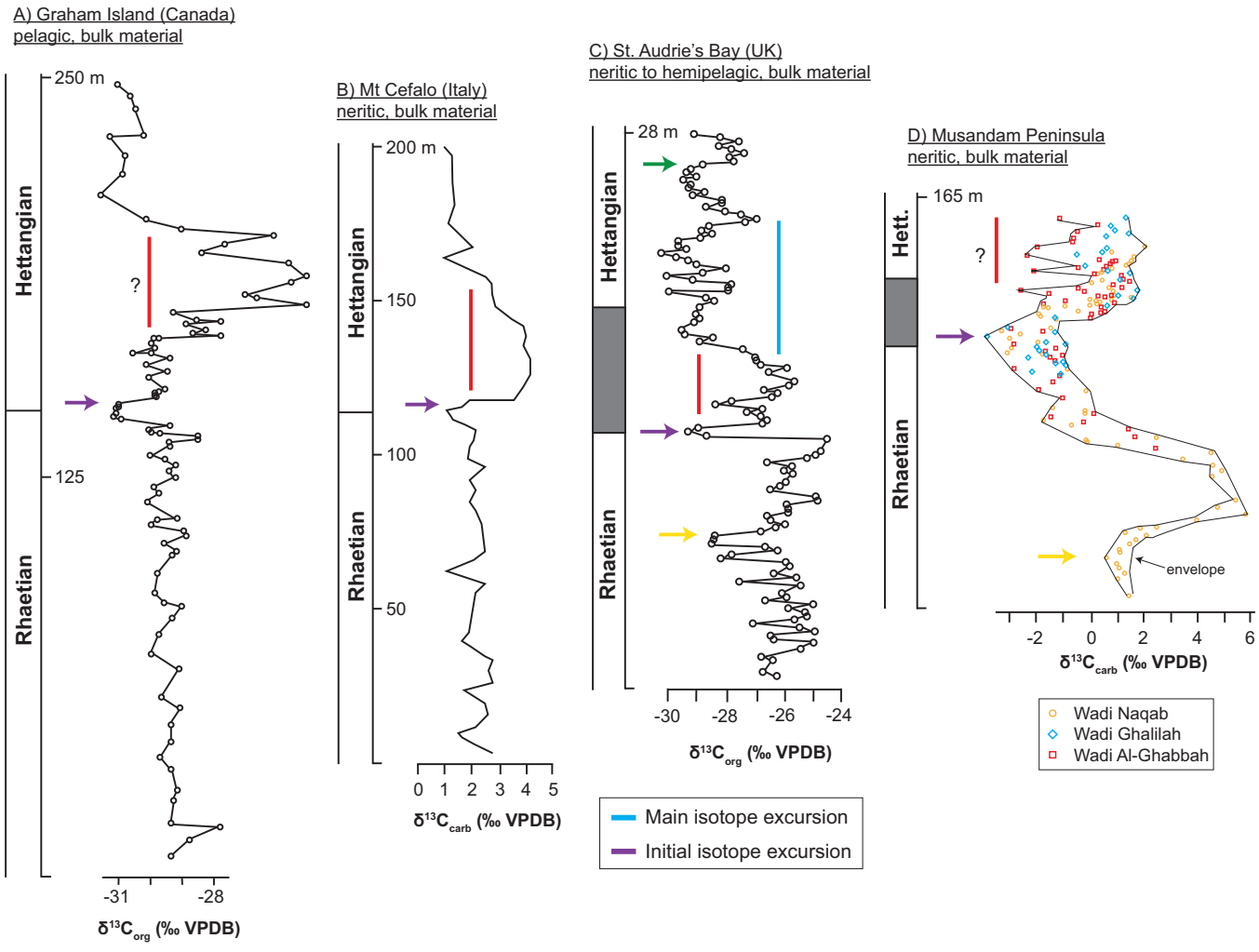
A) Graham Island (Canada)
pelagic, bulk material
250 m
125
Hettangian
Rhaetian
?
-31
-28
δ13Corg (‰ VPDB)
B) Mt Cefalo (Italy)
neritic, bulk material
200 m
150
100
50
Hettangian
Rhaetian
0 1 2 3 4 5
δ13Ccarb (‰ VPDB)
C) St. Audrie's Bay (UK)
neritic to hemipelagic, bulk material
28 m
Hettangian
Rhaetian
-30 -28 -26 -24
δ13Corg (‰ VPDB)
Main isotope excursion
Initial isotope excursion
D) Musandam Peninsula
neritic, bulk material
165 m
Hett.
Rhaetian
?
envelope
-2 0 2 4 6
δ13Ccarb (‰ VPDB)
Wadi Naqab
Wadi Ghalilah
Wadi Al-Ghabbah

Figure 12

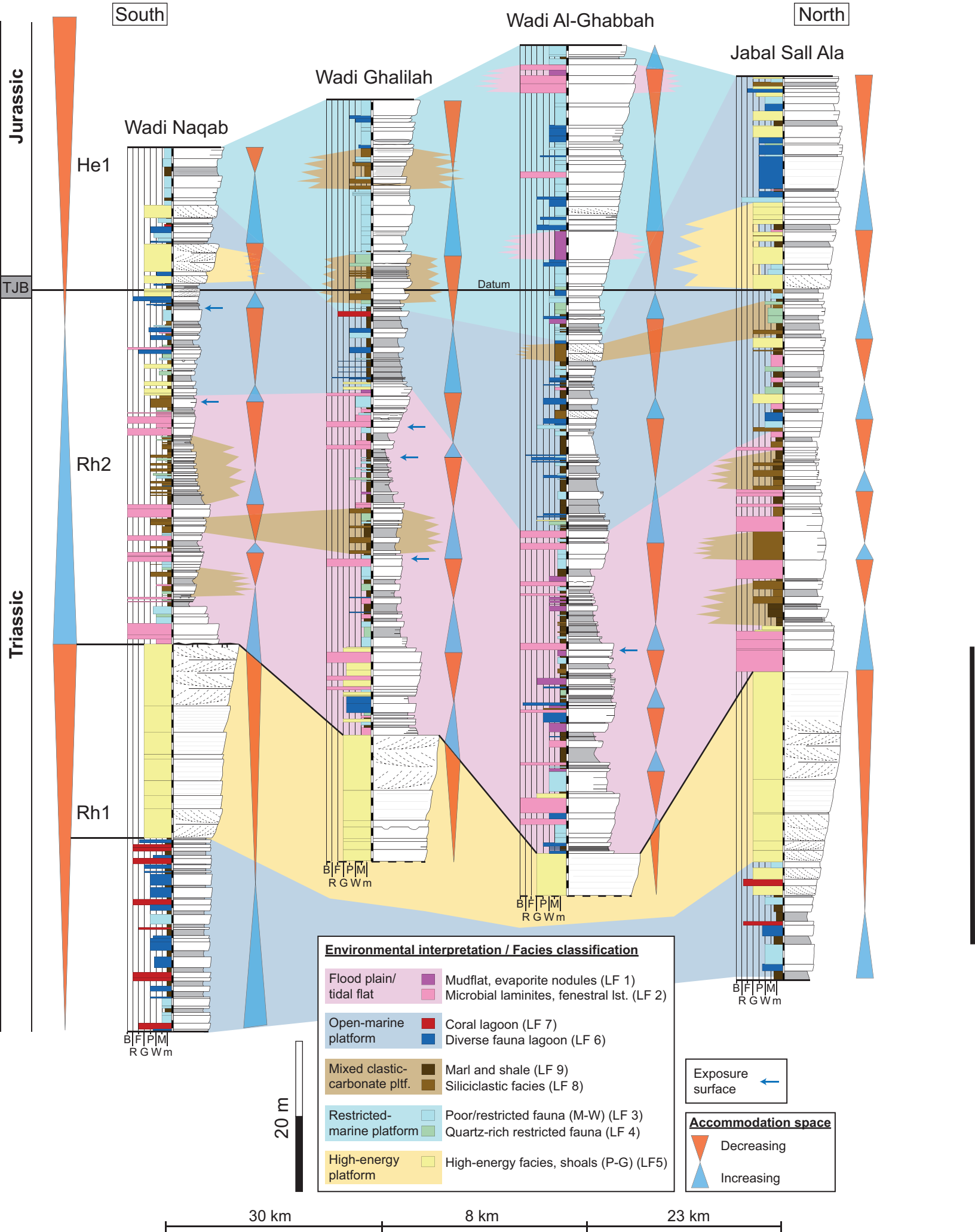
South
North
Wadi Naqab
Wadi Ghalilah
Wadi Al-Ghabbah
Jabal Sall Ala
Jurassic
Triassic
TJB
Datum
He1
Rh2
Rh1
B F P M
R G W m
Environmental interpretation / Facies classification
Flood plain/ tidal flat
Mudflat, evaporite nodules (LF 1)
Microbial laminites, fenestral lst. (LF 2)
Open-marine platform
Coral lagoon (LF 7)
Diverse fauna lagoon (LF 6)
Mixed clastic-carbonate pltf.
Marl and shale (LF 9)
Siliciclastic facies (LF 8)
Restricted-marine platform
Poor/restricted fauna (M-W) (LF 3)
Quartz-rich restricted fauna (LF 4)
High-energy platform
High-energy facies, shoals (P-G) (LF5)
Exposure surface
Accommodation space
Decreasing
Increasing
20 m
30 km
8 km
23 km

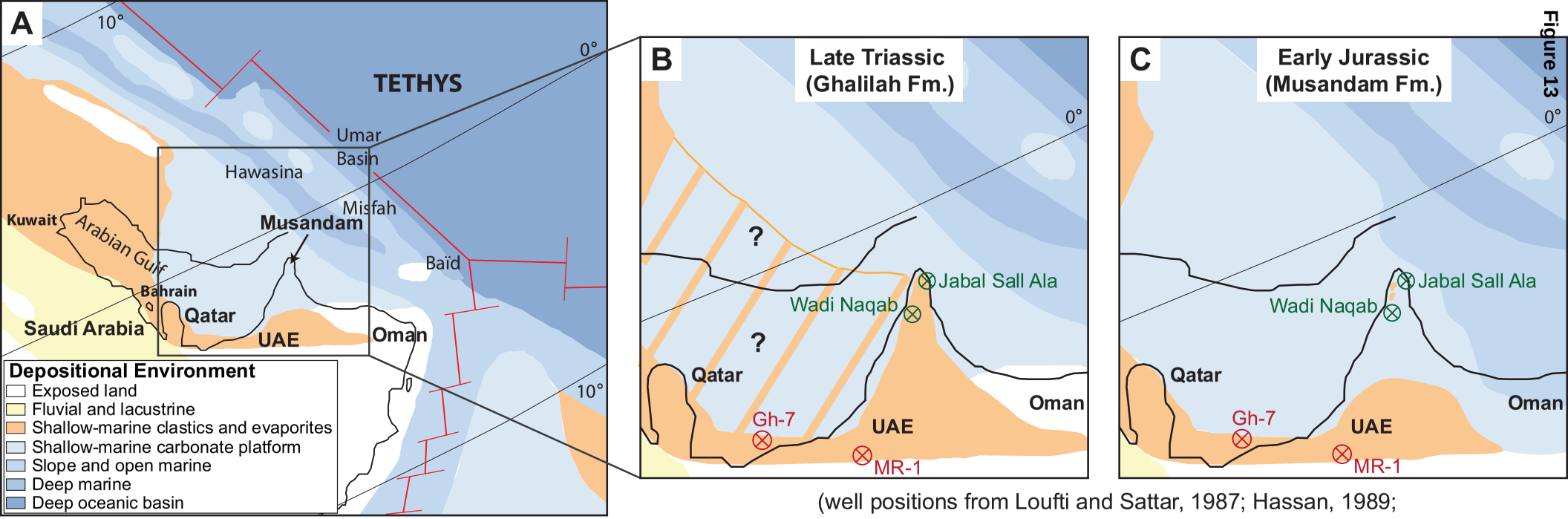

(modified after Al-Husseini, 1997; Ziegler, 2001; Rousseau et al., 2005)

(well positions from Loufti and Sattar, 1987; Hassan, 1989;
in accordance with Bendias and Aigner, 2015)

Figure 13

Figure 14

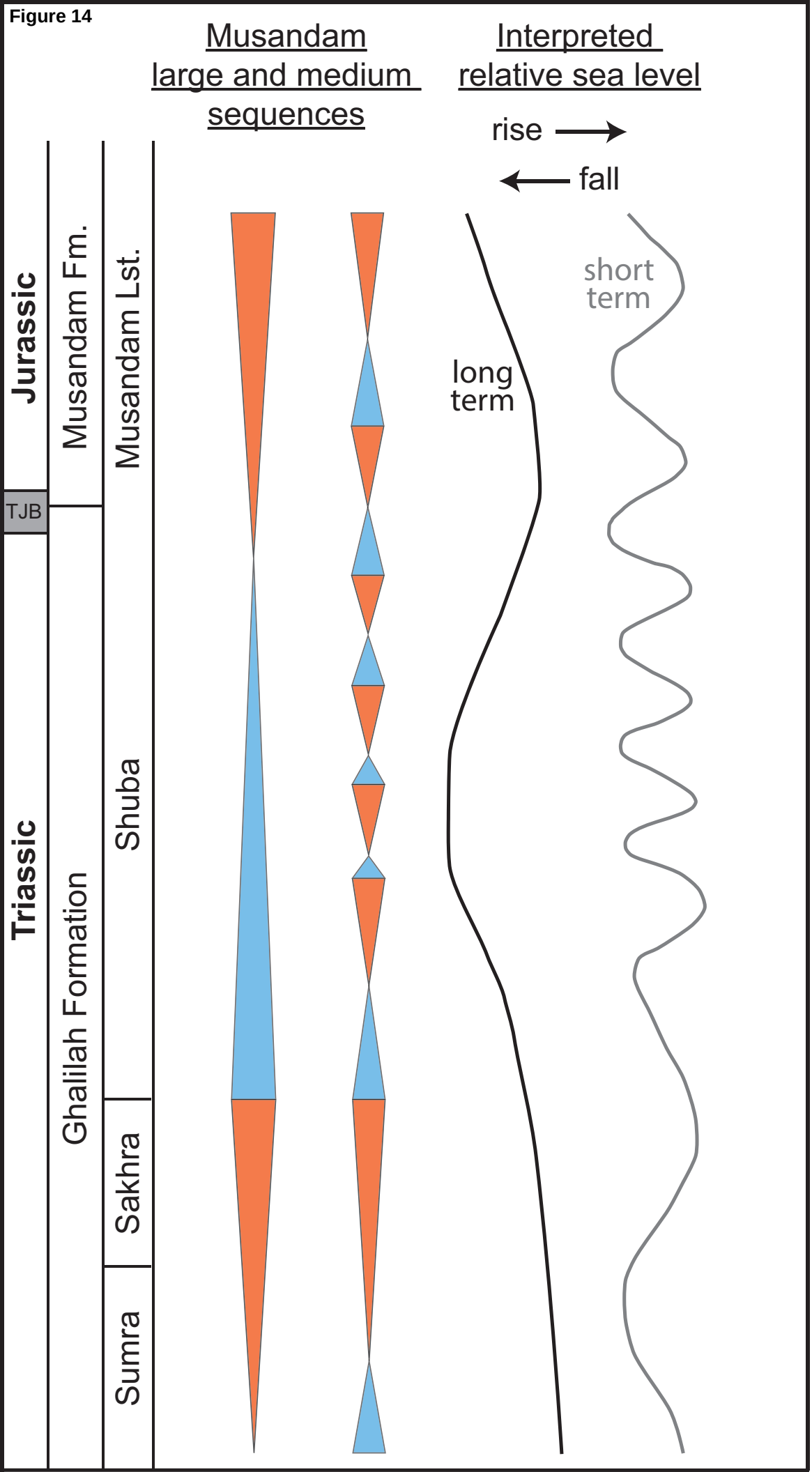
Musandam large and medium sequences
Interpreted relative sea level
rise
fall
short term
long term
Jurassic
Triassic
TJB
Musandam Fm.
Ghalilah Formation
Musandam Lst.
Shuba
Sakhra
Sumra

Table 1

LF	Facies	Dunham Texture	Main Components	Sedimentary Features	Depositional Environment	Dimensions
1	Mudflat facies	M M-W	Fenestrae, peloids, bioclasts fragments, calcite nodules, quartz, mudclasts	Nodules, lamination, mudclasts	Flood plain, maybe tidal flat	Thickness: 0.1 – 3.8 m Max. lateral extent: < 8 km
2	Microbial laminite	B M	Microbial mats, stromatolite, fenestrae, often dolomitised	Domal structures, tepees, mud-streaks, bioturbation (*Skolithos*)	Flood plain, maybe tidal flat or intertidal zone	Thickness: 0.15 – 2 m Max. lateral extent: 46 km
3	Restricted fauna	M W W-P	Bivalves, gastropods, peloids, echinoderms, lithoclasts, ooids	Irregular, nodular bedding, bioturbation	Restricted platform	Thickness: 0.05 – 2.7 m Max. lateral extent: 30 km
4	Quartz-rich restricted fauna	W W-P	Bivalves, quartz, gastropods, ostracods, echinoderms, peloids partly dolomitised	Irregular, nodular, channelised	Restricted platform	Thickness: 0.1 – 1.2 m Max. lateral extent: 23 km
5	High-energy facies	G	Ooids, peloids, bivalves, oysters, lithoclasts, aggregate grains, echinoderms, dasycladacean algae	Cross-lamination and –stratification, mud-drapes	High-energy platform; open marine platform; intertidal zone	Thickness: 0.15 – 26 m Max. lateral extent: 46 km
6	Diverse fauna	P R	Bivalve fragments, gastropods, foraminifera, ostracods, echinoderms, oysters, peloids, coral fragments	Bioturbation (e.g. *Rhizocorallium, Chondrites*)	Open marine platform	Thickness: 0.05 – 3.7 m Max. lateral extent: 46 km
7	Coral facies	R B	Large massive corals, grainy ooidal matrix, gastropods	Bioturbation, vugs	Subtidal zone; open platform	Thickness: 0.2 – 0.9 m Max. lateral extent: 46 km

8	Siliciclastic facies	-	Quartz, calcite-cemented, occasional dolomite cement, conglomerate (monomictic and polymictic)	Cross-lamination and –stratification, nodular bedding, flaser-bedding, red Fe/Mn nodules, lenticular bedding, wave ripples, hummocky cross-stratification	Intertidal zone; open platform	Thickness: 0.1 – 3.8 m Max. lateral extent: 30 km
9	Shale and marl	m	Marls brown-grey, red, green, laminated shales, nodules	Lamination, nodules, bioturbation,(e.g. *Thalassinoides)*	Deep, open platform	Thickness: 0.1 – 3.8 m Max. lateral extent: 30 km

Supplement Isotope data

Click here to download Raw research data (under CC BY license; see above): Supplement Raw isotope data.xlsx